Numerical investigation of response-conditioning wave techniques for short-term rare combined loading scenarios

Seyffert, H. C.; Kana, A. A.; Troesch, A. W.

DOI
10.1016/j.oceaneng.2020.107719

Publication date
2020

Document Version
Final published version

Published in
Ocean Engineering

Citation (APA)
Seyffert, H. C., Kana, A. A., & Troesch, A. W. (2020). Numerical investigation of response-conditioning wave techniques for short-term rare combined loading scenarios. *Ocean Engineering*, *213*, Article 107719. https://doi.org/10.1016/j.oceaneng.2020.107719

Ocean Engineering 213 (2020) 107719

Contents lists available at ScienceDirect

Ocean Engineering

journal homepage: www.elsevier.com/locate/oceaneng

Numerical investigation of response-conditioning wave techniques for short-term rare combined loading scenarios

H.C. Seyffert [a,*], A.A. Kana [a], A.W. Troesch [b]

[a] Department of Maritime & Transport Technology, Delft University of Technology, The Netherlands
[b] Department of Naval Architecture & Marine Engineering, University of Michigan, USA

ARTICLE INFO

Keywords:
Response-conditioned waves
Combined loading
Rare responses
Short-term statistics
Trimaran

ABSTRACT

Response-conditioning wave techniques are a rational way to link wave excitation environments with return-period extreme loading responses. By retaining the wave excitation which leads to a design response, these techniques can also define extreme combined loading scenarios. For complex or novel hull forms, combined loading may be relevant for evaluating structural reliability or adequacy. But using combined loading scenarios as inputs to high-fidelity structural or dynamic modeling tools implies that such load scenarios are realistic for the defined return-period. This paper investigates three response-conditioning wave techniques: a modified Equivalent Design Wave method, a modified Conditioned Random Response Wave method, and the Design Loads Generator, to evaluate how well they reproduce combined loading statistics for a 1000-hr return-period as compared to stochastic brute-force simulations. The investigation is carried out for extreme combined loading scenarios on a 110 m trimaran hull. The Design Loads Generator produces the most realistic extreme combined loading statistics as compared to the brute-force approach with a significant reduction in computation time based on combined load conditional probability density functions, cumulative density functions, and individual stochastic load vectors.

1. Introduction

To ensure adequate lifetime structural performance, many classification societies suggest using combined loading scenarios as possible loading conditions to test a vessel's structural compliance, see, e.g. Lloyd's Register (2017), Bureau Veritas (2018a), DNV-GL (2018), Bureau Veritas (2017, 2018b), American Bureau of Shipping (2016, 2005), IACS (2018), Horn et al. (2013), ClassNK (2013) and Lloyd's Register (2014). The intent of using such combined loading scenarios is to capture the effect of stochastic loads acting in different planes of the vessel. However, defining such loading scenarios is not simple, especially for rare events. Even defining a return period for multivariate extremes can be ambiguous, see, e.g. Feld et al. (2019).

To define simultaneous load effects due to combined loading may require the underlying wave profile which excites these stochastic loads. Rare combined loading scenarios may be associated with long exposure periods, making brute-force simulation techniques, such as Monte Carlo Simulations (MCS) potentially intractable. Multiple Response-Conditioning Wave Techniques (RCWTs), such as the Equivalent Design Wave (EDW), Conditioned Random Response Wave (CRRW), and the Design Loads Generator (DLG), have been developed to construct wave profiles expected to excite specific loading scenarios. These methods are significantly more computationally efficient than MCS because they do not simulate the entire return-period to construct waves that excite return-period extreme load responses. Such efficiency and simplicity have made these methods popular because they can easily be implemented by engineers to define lifetime combined loading scenarios.

It is worth wondering, though, whether the simplicity of some of these techniques comes at the expense of accuracy in defining realistic combined loading scenarios associated with long return-periods. This paper examines that potential trade-off by comparing RCWT-defined short-term rare combined loading scenarios with equivalent scenarios from MCS. The main questions of interest here are: what are the inherent limitations or assumptions associated with these RCWTs? Do these techniques recover the same statistics of lifetime combined loading scenarios that result from a brute-force MCS approach? And how does increasing a safety factor affect these load scenarios? These are timely questions, especially as RCWTs are gaining popularity in industry practice for defining load scenarios to evaluate structural adequacy of vessels, even for novel hull forms like trimarans (see Lloyd's Register (2017)).

* Corresponding author.
E-mail address: H.C.Seyffert@tudelft.nl (H.C. Seyffert).

https://doi.org/10.1016/j.oceaneng.2020.107719
Received 31 July 2019; Accepted 27 June 2020
Available online 18 July 2020

The paper is structured as follows: Section 2 gives some background to the RCWTs examined in this investigation. Section 3 establishes the trimaran case study and benchmarks to compare the combined loading scenarios from the RCWTs with MCS. Sections 4–7 evaluate the techniques via the established benchmarks. Finally, Section 8 discusses the trade-offs between the RCWTs and Section 9 offers some recommendations and conclusions.

2. Response-conditioning wave techniques

This section gives a short background on some response-conditioning techniques which define a wave excitation profile based on a specific load response with a given return period. It is worth acknowledging the many other methods that examine combined loading, including, but certainly not limited to: combination formulas like Turkstra's rule (Turkstra, 1970) or the Ferry Borges–Castanheta method (Ferry-Borges and Castanheta, 1971), load coincidence models (Wen, 1993), point-crossing methods (Huang and Moan, 2008), and cross-spectral methods (Alfred Mohammed et al., 2012, 2016). For a recent investigation of such load combination models and their sensitivity when performing a hull girder reliability analysis, see Piscopo and Scamardella (2019).

This paper, however, only examines a few response-conditioning wave techniques which are chosen based on either their present usage as defined by classification societies (EDW), potential for expanding on these classification society methods (CRRW), or expected accuracy in capturing lifetime conditional loading statistics (DLG). In general, all of these techniques have a similar aim: to construct wave profiles which lead to extreme responses of a defined load scenario. Consider a stochastic wave profile time series $\eta(t)$:

$$\eta(t) = \sum_{j=1}^{N} a_j cos(\omega_j t + \phi_j) \tag{1}$$

where

$a_j = \sqrt{2S(\omega_j)\Delta\omega}$

$S(\omega)$ = single-sided wave energy spectrum

ϕ_j = phase between $-\pi$ and π

If the phases ϕ_j are uniformly distributed between $-\pi$ and π, as the number of frequency components N approaches infinity the random variable H expressed by the random process $\eta(t)$ approaches a Gaussian random variable. In general, RCWTs condition a wave profile expected to lead to a pre-determined response value at a pre-determined time, say $t = 0$. In this case, the phases ϕ_j may not be uniformly distributed between $-\pi$ and π but will likely be tuned based on a transfer function of the desired response. Consider now some response of interest $y(t)$ which is excited by the wave elevation $\eta(t)$, expressed as:

$$y(t) = \sum_{j=1}^{N} a_j H_j cos(\omega_j t + \phi_j + \psi_j) \tag{2}$$

where

$a_j = \sqrt{2S(\omega_j)\Delta\omega}$

$S(\omega)$ = single-sided wave energy spectrum

H_j = value of the transfer function relating the wave excitation and the process $y(t)$ at ω_j

ϕ_j = wave phase between $-\pi$ and π from Eq. (1)

ψ_j = process $y(t)$ transfer function phase at ω_j

The random variable Y similarly approaches a Gaussian random variable as N approaches infinity and if ϕ_j are uniformly distributed between $-\pi$ and π. The RCWTs focus on defining the wave phases ϕ_j such that the resulting $y(t = 0)$ response is a rare occurrence. Of course, Eqs. (1)–(2) are linear relationships, but in general, response conditioning wave techniques are based upon linear theory and the assumption that a nonlinear response is a correction of the associated linear response. It is expected, though, that the processes employed in this investigation and conclusions would be similar for nonlinear, non-Gaussian models.

2.1. Equivalent design waves

Equivalent Design Waves are regular waves constructed to lead to a specific load value, here referred to as a design value, in a given heading at a specified instant in time, again at $t = 0$. To define a load combination case, a single load is chosen as the primary load, called M_p, which is the load the EDW is constructed to maximize. This EDW is constructed using the response amplitude operator (transfer function) of M_p ($RAO_{M_p}(\omega_e)$) in a particular heading. The frequency of the EDW, called ω_{e^*}, is the encounter frequency corresponding to the peak value of $RAO_{M_p}(\omega_e)$. By construction, the EDW and resulting load profiles are regular waves with this same frequency ω_{e^*}. The value of the primary load RAO and phase at this frequency ω_{e^*} are used to define the resulting EDW. Interested readers are referred to Seyffert and Kana (2019) and Seyffert et al. (2018) for more discussion on the implementation of the EDW technique for this investigation.

2.1.1. Implications of EDW assumption

The major assumption of the EDW method is that the wave which excites a specified loading scenario is regular and that the resulting loads are regular waves with the same frequency. This makes for a very simple construction of the EDW and resulting load profiles but means that the resulting load profiles have a limited range. Consider a vector of time-varying load profiles excited by an EDW. Since all of the load profiles are phase-shifted cosines with the same frequency ω_{e^*}, the implication is that the combined load vector in n-dimensional space (each dimension relating to a specific global load) will be a $2-d$ ellipse.

The shape of an EDW-driven load vector is pre-determined because any phase-shifted cosine with a given frequency can be represented as a weighted linear combination of a sine and cosine wave at that same frequency. For load vectors excited by an EDW, this means that the range of an n-dimensional load vector excited by an EDW has the maximum dimension of 2. Graphically, an n-dimensional load vector excited by an EDW plotted in n-dimensional space will trace out an ellipse which lies on a $2-d$ plane. The range of that ellipse has dimension 2 and the null-space has dimension $n-2$, regardless of the number of loads n excited by the EDW.[1] The major question for evaluating the EDW as a response-conditioning wave technique is then: do the limitations stemming from the regular wave assumption outweigh the simplicity of application? Can the EDW lead to realistic combined loading scenarios as compared to more complex RCWTs and the benchmark MCS?

2.2. New waves, most-likely waves, and conditioned random response waves

Many response-conditioning wave techniques have been developed to take the general idea of the EDW (to construct a wave which leads to

[1] Consider the set of functions V on $\mathbb{R}$ that are a sum of a sine and cosine wave with the same frequency: i.e. $Asin(x) + Bcos(x)$, where A and B are real constants. V is a vector space because linear sums of elements of V and scalar multiples of elements of V are also members of V. Since $sin(x)$ and $cos(x)$ are maximally linearly independent in V, meaning that there are no other linearly independent functions in the vector space V, they form a basis of V. The implication of this is that a vector of n combined loads excited by an EDW has at maximum 2 linearly independent dimensions. Such results can readily be confirmed from linear algebra or signal processing textbooks, see, e.g. Smith (2002). Indeed, the fact that $sin(x)$ and $cos(x)$ form a basis of V is an underpinning of the Fourier series.

an extreme system response of interest) and correct for its shortcomings (namely, that the EDW is a regular wave). These techniques do not determine such wave profiles via brute-force simulation techniques but rather linear and probabilistic theory based on expectations of wave profiles given certain conditional criteria. Lindgren introduced the New Wave profile, giving a form for the expected (i.e. most-likely) profile of a Gaussian process conditioned on an extreme peak value at a given time instant (Lindgren, 1970); this result was also demonstrated by Tromans et al. (1991). Friis-Hansen and Nielsen developed the Most-Likely Wave (MLW) by expanding the New Wave profile to condition on both the wave amplitude and instantaneous frequency (Friis-Hansen and Nielsen, 1995). If this instantaneous frequency is the mean frequency $\omega = m_1/m_0$, where m_i is the ith moment of the wave energy spectrum, the MLW simplifies to the New Wave profile.

But since this New Wave profile is simply the autocorrelation function of the wave spectrum, Taylor et al. added randomness to the expression by embedding this most-likely wave profile into a random seaway (Taylor et al., 1997). However, a single extreme wave crest may not excite extreme dynamic responses. Airy wave theory suggests that the wave leading to the worst-case system response is the one which excites a response where all frequency components have a peak at the same time. Torhaug developed the Critical Wave Episode model which identifies wave profiles via a linear model that are expected to lead to extreme system responses. This model uses simulations based on design sea state histories to screen for critical wave characteristics (Torhaug, 1996). For example, a critical wave characteristic might be extreme wave height, meaning that the constructed Critical Wave Episode is based on the New Wave model.

Other authors have constructed wave profiles which lead to specific vessel responses by using the linear transfer function that links the wave excitation and response. Dietz combined the Most-Likely Wave (MLW) profile from Friis-Hansen and Nielsen with the Most-Likely Extreme Response (MLER) method from Adegeest et al. (1998) to develop the Most-Likely Response Wave (MLRW) (Dietz, 2004). The deterministic MLRW is conditioned on a linear vessel response taking a specified extreme value at a given instant in time with a given instantaneous frequency. If this instantaneous frequency is the mean frequency, the MLRW is the same as the MLER wave. When this MLRW/ MLER wave includes a random background, it is referred to as a Conditioned Random Response Wave (CRRW).

The MLWR (and therefore the CRRW) is similar to the EDW approach in that the linear response transfer function defines the resulting phase of the conditioned wave component at each frequency component. The MLRW uses the range of frequencies from the response transfer function, instead of the peak frequency like the EDW, to define the amplitude of each wave component. The MLRW incorporates the envelope process of the response along with an instantaneous frequency requirement at the time of the response event. The CRRW further includes normally distributed coefficients in the wave amplitudes, leading to an irregular wave profile. The details of the derivation of the CRRW can be found in Dietz (2004); the formulation of the CRRW technique employed here follows Drummen et al. (2009). It is worth noting, though, that the CRRW does not include randomness in the extreme loading event itself as this value is fixed *a priori*.

2.3. Generating a distribution of extreme responses from EDW & CRRW

By construction the EDW and CRRW techniques are designed to lead to a single *a priori* defined load value. While the CRRW includes randomness in the constructed wave profile, there is no randomness included in the extreme load response of interest at $t = 0$. In reality though, a vessel experiences a distribution of extreme loading based on the exposure time in the operational profile. This is reflected when running MCS and in waves constructed by the Design Loads Generator, as discussed in the next section (Section 2.4): a distribution of extreme responses is collected. To compare with the DLG and MCS, the EDW and CRRW techniques are adjusted to construct an ensemble of waves which lead to a distribution of extreme load values.

A closed-form distribution can be defined for extreme values of a Gaussian process given its zero-crossing period and the return-period. Then, an ensemble of extreme load values can be chosen such that their empirical histogram approaches the theoretical Gaussian extreme value distribution (EVD) for the defined exposure. As deep-water waves can be assumed Gaussian and the loading transfer functions are linear, this is a reasonable estimation of the extreme loading distribution. This logic constructs the DLG wave profiles: an ensemble of waves that lead to a distribution of extreme responses whose empirical histogram approaches the Gaussian EVD. Based on this ensemble of extreme load values which follow the Gaussian EVD, an ensemble of Equivalent Design Waves and Conditioned Random Response Waves can be constructed which excite these load values. This approach distinguishes the modified-EDW (m-EDW) and modified-CRRW (m-CRRW) approaches used in this investigation. This modification allows a direct comparison between the m-EDW, m-CRRW, DLG, and MCS approaches for the different combined loading scenarios considered, as all RCWTs construct ensembles of waves leading to distributions of extreme load responses.

2.4. Design loads generator

The DLG was developed to construct an ensemble of irregular wave profiles which are expected to lead to extreme return-period linear system responses based on a loading transfer function and an exposure time (Alford, 2008; Kim, 2012). Unlike the response-conditioning wave techniques discussed in the previous subsections, the DLG does not fix the extreme load value *a priori* and then back-calculate a wave profile which leads to this response based on summing phase-shifted regular wave components via Airy wave theory. Instead, the question that drove the development of the DLG was: what is the distribution of wave phases ϕ_j in Eq. (1) that leads to extreme responses of $y(t)$ at time $t = 0$ which belong to the Gaussian EVD for a given exposure? The main differences between the RCWTs discussed earlier and the DLG are:

- The DLG does not require an *a priori* definition of the extreme load value at $t = 0$ to construct the underlying wave profile, unlike EDW and CRRW. The extreme load value excited by a DLG wave is by construction a member of the Gaussian EVD for the defined exposure period. The DLG constructs an ensemble of short irregular wave profiles which excite extreme return-period response values which belong to the theoretical Gaussian EVD based on a characteristics period of the response (e.g. zero-crossing period) and the return-period.
- The phases ϕ_j in Eq. (1) of the DLG waves are not limited based on the phases of the associated linear transfer function which describes the response of interest.
  - The EDW can be seen as a simplification of Eq. (1) where only the frequency ω_{e^*} which corresponds to the peak of the load RAO_{M_p} is included and where the height of this wave is scaled to lead to a specific design value. By construction then, the EDW wave phase ϕ_j is defined by the transfer function phase at the frequency ω_{e^*}, $-\psi_j$.
  - The MLRW/ CRRW wave uses more frequency components than the EDW and conditions based on an instantaneous frequency, but also has the phase of each regular wave component defined completely by the load transfer function; i.e. $\phi_j = -\psi_j$. Therefore, both EDW and CRRW construct waves with phases at each frequency component which only take on values contained in the range of phases in the load transfer function. In contrast, the DLG wave components at each frequency can take phases between $-\pi$ and π.

Table 1
Trimaran parameters & operational profile.

Parameter	Value
Hull overall length (LOA)	110.0 m
Hull waterline length (L)	106.4 m
Total Draft	4.897 m
Beam	30.48 m
Vessel mass	3,301,440 kg
Num. wave frequency components	100
Speed, Froude number	12.803 m/s, 0.4
Spectrum type	Bretschneider (H_s, T_m)
Significant wave height (H_s)	12.5 m
Modal period (T_m)	9.5 sec
Exposure	1000-h

3. Case study: Trimaran

For the numerical investigation of how well different response-conditioning wave techniques describe lifetime combined loading scenarios, a trimaran hull is examined. Combined loading is relevant for trimaran structural design, especially the cross deck structure. Increasing advances in high-fidelity structural modeling allow an in-depth study of such complex structural responses. But the limited historical and anecdotal knowledge about trimarans makes efficiently applying such models difficult. Therefore, response conditioning wave techniques may be relevant to define a finite number of lifetime combined loading scenarios for use in such tools. Indeed, some classification societies have already suggested this procedure to evaluate the adequacy of trimaran structures, e.g. Lloyd's Register (2017).

To compare load combination scenarios defined by the different RCWTs, the trimaran hull is the same as used in Seyffert and Kana (2019), Seyffert et al. (2018), which examined combined loading scenarios defined by the EDW technique. The trimaran parameters and operational profile for the load scenarios are given in Table 1. For this analysis, the rareness of the load combinations is limited by the exposure period which can reasonably be simulated by MCS to give converged statistics. Therefore, the chosen exposure time is 1000-h. Although a designer may be interested in rarer combined loading events, it is relevant to evaluate whether the RCWTs accurately describe load scenarios at a shorter return-period like 1000-h. It is not expected that EDW or CRRW will become more accurate for describing rarer responses or for flexible hulls where non-linearities will be more dominant, as compared to brute force stochastic simulations or physical model tests, see, e.g. Drummen et al. (2009). The DLG waves will still be statistically valid for events associated with longer return-periods, as any return-period can be related to a Gaussian EVD, though the Gaussian process assumption may break down for such rare responses due to non-linearities.

3.1. Combined loading scenarios on a Trimaran

Typically combined loading scenarios are based on conditional maxima. For all of the techniques described in Section 2, the load scenarios are defined by the simultaneous responses of all loads when a specific global load attains its 1000-h extreme value. These global loads are defined in Fig. 1. The vertical wave bending moment, M_W, is the wave pressure distribution integrated across the depth of the vessel and the horizontal bending moment, M_H, is the pressure distribution integrated across the vessel breadth.

M_W = vertical wave bending moment

M_{SP} = splitting bending moment

M_{LT} = longitudinal torsional bending moment

M_H = horizontal bending moment

M_{TT} = transverse torsional bending moment

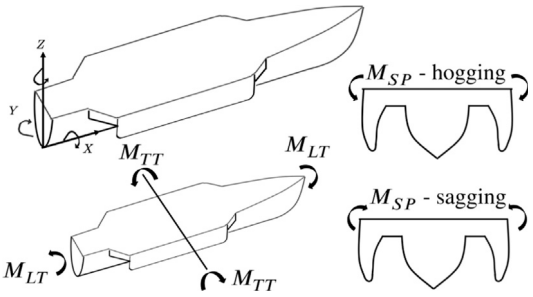

Fig. 1. Trimaran coordinate system (Seyffert and Kana, 2019; Seyffert et al., 2018).

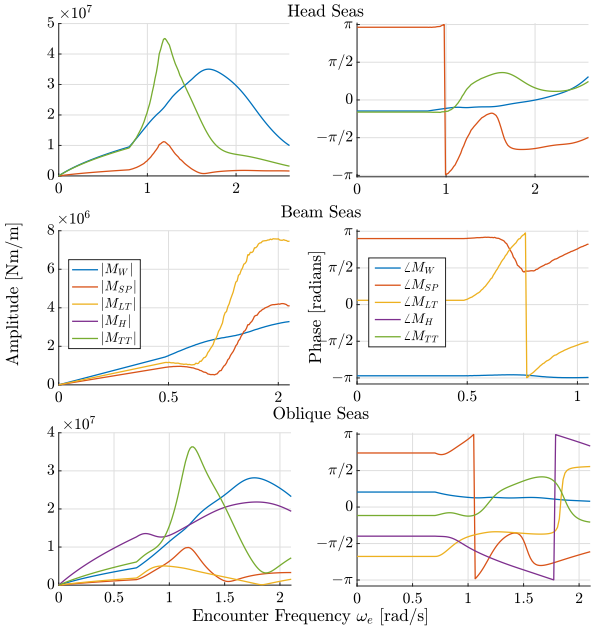

Fig. 2. Load transfer functions.

For this investigation, combined load scenarios are defined when each of the global loads in Fig. 1 attains its extreme value in a given heading. The linear version of the high-order potential flow code Aegir (Kring et al., 2004) was used to generate the trimaran transfer functions of the global loads. These transfer functions are adapted from Seyffert and Kana (2019) and Seyffert et al. (2018), where the minimum earth-coordinate frequency was $\omega_0 = 0.4859$ rad/s. Here, the transfer functions are linearly extrapolated so that the minimum frequency is $\omega_0 = 0$ rad/s. The amplitudes are linearly extrapolated so that the amplitude at $\omega_0 = 0$ rad/s is zero. The phases are extrapolated so that all phases at $\omega_0 \leq 0.4859$ rad/s equal the transfer function phase at $\omega_0 = 0.4859$ rad/s. This extrapolation is necessary to conduct MCS to examine lifetime loading scenarios. The MCS analysis uses the Fast Fourier Transform (fft) algorithm to simulate the stochastic ocean environment. The fft algorithm assumes the frequency range begins from $\omega_0 = 0$ rad/s, requiring the extrapolation for this investigation. The extrapolated transfer functions are shown in Fig. 2.

3.2. Design values of global loads

As described in Seyffert and Kana (2019) and Seyffert et al. (2018), the heading of each load scenario is based on the heading where the specific global load attains its largest 1000-h extreme value. In each heading, the most-likely extreme value of each load is determined using extreme value theory, see, e.g. Ochi (1990), with a zero-crossing

Table 2
Most-likely 1000-h extreme value for each load in each heading given the operational profile from Table 1. The design values are the largest most-likely extreme values over all headings, and are shown in bold.

Load	Most-likely extreme value, given heading		
	Head seas	Beam seas	Oblique seas
M_W	**3.890e8 Nm**	3.589e7 Nm	2.783e8 Nm
M_{SP}	8.151e07 Nm	3.190e7 Nm	**8.240e7 Nm**
M_{LT}	–	**6.521e7 Nm**	5.295e7 Nm
M_H	–	–	**2.557e8 Nm**
M_{TT}	**3.804e08 Nm**	–	3.158e8 Nm

period based on spectral moments. These 1000-h most-likely extreme values based on heading are given in Table 2. The largest most-likely extreme value of a load M_i over all the headings is defined as the design value R_{M_i}, and given in bold. Not all transfer functions were constructed for all headings. In those cases, the most-likely extreme value for that load case is marked as "–". Load combination factors, or *LCF*s, can be defined as the resulting load combination where each load is normalized by its respective design value.

3.3. Evaluating RCWT-defined lifetime combined loading scenarios

Defining realistic combined loading scenarios is of vital importance for an adequate structural design of novel vessels like trimarans. If these load scenarios are used in high-fidelity modeling tools to assess a design's structural adequacy, it is important that these load scenarios are statistically relevant and physically realistic. The main question is then: does it matter which technique is used to define these load scenarios (m-EDW, m-CRRW, DLG, MCS)? Do all of these methods give comparable statistics of lifetime combined loading scenarios? Clearly, any load combinations derived from statistics of brute-force MCS associated with the desired exposure period will be the most realistic because these situations are not based on any load conditioning, only the system physics as described in the stochastic simulations.

While a brute-force MCS approach is not a feasible approach for daily use by engineers to define lifetime load combinations, it can certainly be used as a benchmark to compare the other techniques. For each heading, 500, 1000-h MCS are run and statistics on the conditional maxima for each global load in Fig. 1 are collected in the headings suggested by Table 2. As well, the wave profile and resulting load vector time series around the time of the 1000-h maximum of each global load is saved for later comparison with the m-EDW, m-CRRW, and DLG analyses. The points of comparison between these techniques will be:

1. How do conditional probability density functions (*pdf*'s) for each load case defined by the RCWTs compare with MCS (Section 4)? This comparison will give good insight on whether the RCWTs accurately describe the relative magnitude and variance of the extreme combined loading distributions for this trimaran hull to evaluate the potential variation in short-term extreme combined loading scenarios.
2. How do conditional cumulative density functions (*cdf*'s) for each load case defined by the RCWTs compare with MCS (Section 5)? This comparison can illustrate the risk factors associated with these load scenarios, and whether increasing the risk factor on the primary load in a load case affects all loads equally.
3. How do load vectors associated with the most-likely 1000-h extreme primary load response from the RCWTs compare with MCS (Section 6)? This comparison will give insight on the simultaneous load correlations excited by the RCWTs.
4. What is the computational effort associated with employing RCWTs versus MCS (Section 7)? This comparison will help balance the simplicity and efficiency of applying the RCWTs with the quality of the resulting combined load scenarios.

4. Conditional *pdf's* from RCWTs vs. MCS

The first way to compare the RCWTs in terms of defining realistic combined loading scenarios is by considering the conditional *pdf*'s assembled by each technique for each case. In each case, a single global load called the primary load M_p is maximized at time $t = 0$ in the heading directed by the design values in Table 2. The different RCWTs (m-EDW, m-CRRW, DLG) assemble wave profiles which lead to 500 $M_p(t = 0)$ values belonging to the Gaussian EVD where R_{M_p} is the 1000-h most-likely extreme value for the operational profile in Table 1. These resulting wave profiles can be used to assemble distributions of all $M_i(t = 0)$ responses conditioned on the extreme $M_p(t = 0)$ events. To describe these conditional *pdf*'s constructed by the different RCWTs and by MCS, the nomenclature in Eq. (3) in Box I is used.

By construction then, all RCWTs will lead to a 1000-h extreme value $M_p(t = 0)$ distribution with a most-likely extreme value at the load design value (i.e. $LCF = 1$). Based on the conditioning technique, the conditional $M_i(t = 0)$ distributions will differ. The load *pdf*'s from the RCWTs and MCS are compared when normalized both as a LCF and in physical dimensions to illustrate how well the RCWTs capture the potential load variance for the different cases.

4.1. Head seas

In head seas, both M_W and M_{TT} experience their design value. Conditional *pdf*'s based on 1000-h extreme $M_W(t = 0)$ and $M_{TT}(t = 0)$ responses in head seas are shown in Figs. 3(a)–3(b), respectively. From Figs. 3(a)–3(b), it is clear that the conditional *pdf*'s from the DLG prove the best visual match with the conditional *pdf*'s from MCS. The $f_i^{\text{m-CRRW}}(M_i|M_W)_H$ and $f_i^{\text{m-CRRW}}(M_i|M_{TT})_H$ distributions overestimate the respective MCS distributions (positive $f_{TT}^{\text{m-CRRW}}(M_{TT}|M_W)_H$ and negative $f_{SP}^{\text{m-CRRW}}(M_{SP}|M_W)_H$ and positive $f_W^{\text{m-CRRW}}(M_W|M_{TT})_H$ and negative $f_{SP}^{\text{m-CRRW}}(M_{SP}|M_{TT})_H$). In contrast, $f_i^{\text{m-EDW}}(M_i|M_W)_H$ and $f_i^{\text{m-EDW}}(M_i|M_{TT})_H$ do not exhibit any single trend when compared with MCS. The m-EDW method under-predicts $f_{TT}^{\text{MCS}}(M_{TT}|M_W)_H$, but $f_{SP}^{\text{m-EDW}}(M_{SP}|M_W)_H$ is centered around $LCF = 0$ like the respective MCS distribution. However, $f_{SP}^{EDW}(M_{SP}|M_W)_H$ is extremely narrow, unlike the respective distributions from the DLG, m-CRRW, and MCS. This result is not surprising, though, when considering the construction of m-EDW waves. The m-EDW waves conditioned to maximize $M_W(t = 0)$ have the frequency $\omega_e = 1.69$ rad/s. At this frequency, the phase difference between M_W and M_{SP} is about $\pi/2$ radians. When M_W is maximized at $t = 0$ by the EDW, M_{SP} is almost $\pi/2$ radians out-of-phase with the M_W response, resulting in a load distribution at $t = 0$ centered around $LCF = 0$ with low variance.

4.2. Beam seas

In beam seas, only M_{LT} experiences its design value. Conditional *pdf*'s based on 1000-h extreme $M_{LT}(t = 0)$ responses in beam seas are shown in Fig. 4. All of the RCWTs give reasonable estimates of the MCS *pdf*'s conditioned on extreme $M_{LT}(t = 0)$ responses in beam seas as compared to MCS. All techniques indicate that $f_W(M_W|M_{LT})_B$ is marginally positive and close to $LCF = 0$. The m-EDW technique seems to slightly over-estimate the peak of the $f_{SP}(M_{SP}|M_{LT})_B$ response distribution.

4.3. Oblique seas

In oblique seas, both M_{SP} and M_H experience their design value. Conditional *pdf*'s based on 1000-h extreme $M_{SP}(t = 0)$ and $M_H(t = 0)$ responses in oblique seas are shown in Figs. 5(a)–5(b), respectively. There are some striking differences between the $f_i(M_i|M_{SP})_O$ (Fig. 5(a)) and $f_i(M_i|M_H)_O$ (Fig. 5(b)) distributions assembled by the RCWTs and by MCS. The $f_i^{\text{m-EDW}}(M_i|M_{SP})_O$ and $f_i^{\text{m-EDW}}(M_i|M_H)_O$

$f_i^{\text{m-EDW/ m-CRRW/ DLG/ MCS}}(M_i|M_p)_{H/B/O} \equiv pdf$ of $M_i(t=0)$ values conditioned on maximum $M_p(t=0)$ values in head/ beam/ oblique (H/ B/ O) seas constructed by m-EDW/ m-CRRW/ DLG/ MCS (3)

$F_i^{\text{m-EDW/ m-CRRW/ DLG/ MCS}}(M_i|M_p)_{H/B/O} \equiv cdf$ of $M_i(t=0)$ values conditioned on maximum $M_p(t=0)$ values in head/ beam/ oblique (H/ B/ O) seas constructed by m-EDW/ m-CRRW/ DLG/ MCS (4)

Box I.

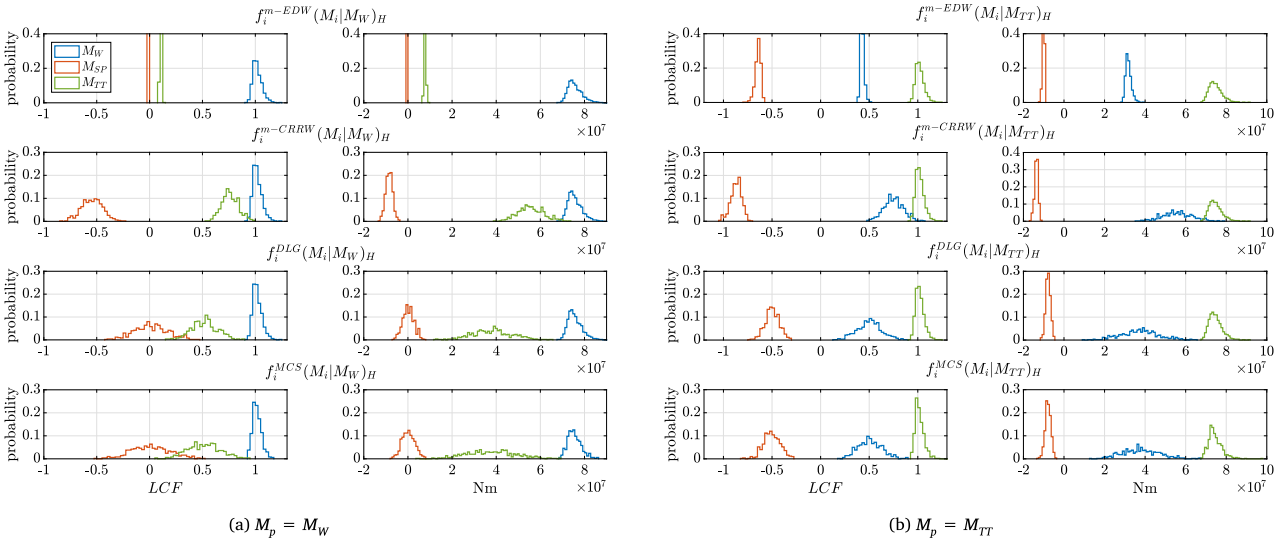

(a) $M_p = M_W$ (b) $M_p = M_{TT}$

Fig. 3. Load *pdf*'s conditioned on maximum $M_p(t=0)$ response in head seas (500 samples as a LCF, left column; Nm, right column).

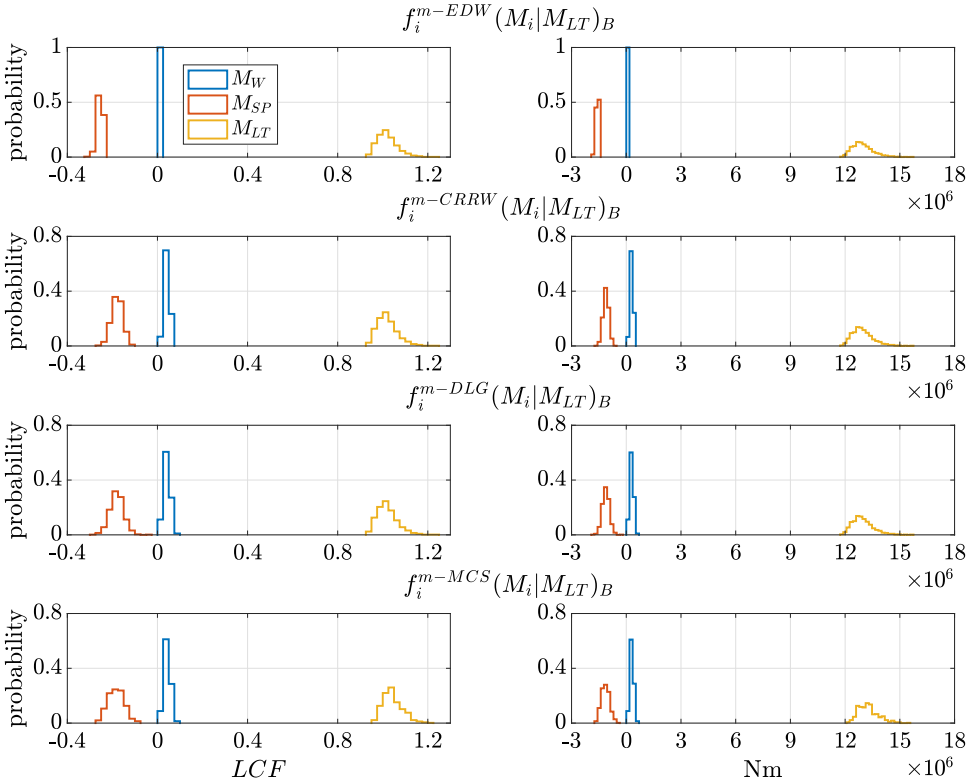

Fig. 4. Load *pdf*'s conditioned on maximum $M_{LT}(t=0)$ response in beam seas (500 samples as a LCF, left column; Nm, right column).

distributions are significantly narrower than the respective MCS distributions, although they do generally track the relative magnitude of the MCS distributions. The m-CRRW technique tracks the relative variance of the MCS distributions but in some instances noticeably over-predicts the load magnitude (negative $f_{TT}^{\text{m-CRRW}}(M_{TT}|M_{SP})_O$ and negative $f_{LT}^{\text{m-CRRW}}(M_{LT}|M_{SP})_O$) or under-predicts that load magnitude ($f_{TT}^{\text{m-CRRW}}(M_{TT}|M_H)_O$).

The most surprising difference when comparing the RCWT and MCS conditional *pdf*'s is that the m-CRRW technique predicts the incorrect sign for both $f_H(M_H|M_{SP})_O$ and $f_{SP}(M_{SP}|M_H)_O$ as compared to MCS. This sign difference from m-CRRW for these loads may be explained by the phase restriction of the m-CRRW based on the range of the load transfer function phases. Fig. 2 indicates that M_{SP} and M_H are nearly π radians out-of-phase for about half of the frequency components: $0 \leq \omega_e \leq 0.7$. Based on the m-CRRW construction then, where the regular wave components have phases defined by the load transfer function phases (i.e. $\phi_j = -\psi_j$), a significant portion of these regular wave components phased to maximize $M_{SP}(t = 0)$ in oblique seas will excite simultaneous negative $M_H(t = 0)$ responses, and vice-versa. This can explain why m-CRRW suggests the conditional extreme $M_{SP}(t = 0)$ and $M_H(t = 0)$ responses have opposite signs. The m-EDW approach also has this phase limitation, but only for a single frequency based on the peak of the primary load *RAO*. It is worth reiterating, though, that all RCWTs as well as MCS use the same transfer functions from Fig. 2. The DLG and MCS do not limit the wave phases ϕ_j in Eq. (1) based on the range of the transfer function phases like m-CRRW and m-EDW.

5. Conditional *cdf's* from RCWTs vs. MCS

The conditional load *pdf*'s assembled by the RCWTs and by MCS in Figs. 3(a)–5(b) do not explicitly link the simultaneous global load values at time $t = 0$. Therefore, conditional *cdf*'s from the RCWTs and MCS are examined, with the nomenclature defined in Eq. (4) in Box I. For clarity, only 50 samples are included in each conditional *cdf*. These 50 samples are at equally spaced probability of non-exceedance, PNE, intervals within the primary load extreme values excited by the 500 m-EDW, m-CRRW, DLG, and MCS wave profiles.

5.1. Head seas

Fig. 6(a) shows the *cdf*'s from the RCWTs conditioned on 1000-h extreme $M_W(t = 0)$ responses in head seas, while Fig. 6(b) shows the *cdf*'s conditioned on 1000-h extreme $M_{TT}(t = 0)$ responses in head seas. The conditional *cdf*'s constructed by m-EDW shown in Figs. 6(a)–6(b) are monotonic towards larger load values (either with positive or negative sign convention) with increasing probability of non-exceedance, PNE. This is unsurprising considering that the ensemble of waves constructed by m-EDW only differ by the wave height, which is tuned to excite a specific primary load value. The wave phase remains the same across all waves constructed by the m-EDW technique.

In contrast, m-CRRW, DLG, and MCS result in non-monotonic conditional *cdf*'s with respect to increasing PNE. Whereas the m-CRRW regular wave phases remain unchanged for the frequency components across the ensemble of constructed waves, random coefficients stochastically alter the wave amplitudes, leading to the non-monotonic conditional *cdf*'s. When the randomness is not included in the CRRW (i.e. reverting back to the MLRW), the resulting conditional *cdf*'s are monotonic with increasing PNE. As a way to quantitatively compare the RCWT and MCS *cdf*'s, conditioned on maximized $M_W(t = 0)$ in head seas, consider Figs. 7(a)–7(b).

Fig. 7(a) examines the percentage of conditional *cdf* values assembled by each RCWT that are within some error bound of the respective MCS conditional *cdf*, with this bound measured as a percentage of each load's design value, considering all 500 extreme load responses. If a RCWT *cdf* were exactly the same as the MCS conditional *cdf*, 100% of its *cdf* values would have a 0% difference from the design value of the MCS *cdf*. This comparison considers how well the RCWT conditional *cdf* matches the MCS conditional *cdf* on a global sense. The RCWT leading to the best fit with MCS will have the highest percentage of its conditional *cdf* values within the smallest percentage difference from the respective MCS *cdf* (i.e. fastest ascent to 100 on the y-axis). Fig. 7(b) compares the RCWT and MCS conditional *cdf*'s on a more point-by-point basis by examining the LCF difference between the conditional *cdf*'s at the 50 PNE values included in the conditional *cdf*'s. In this case the RCWT leading to the best fit with MCS will have the minimum difference at each sampled PNE value. A perfect fit with the MCS *cdf* would result in zero difference at each PNE value.

Fig. 7(a) indicates that the RCWT *cdf*'s conditioned on maximized $M_W(t = 0)$ in head seas all have 100% of their samples within 3% of R_{M_W} from the MCS *cdf*. Since by construction all RCWTs lead to a distribution of $M_W(t = 0)$ values which follow the 1000-h Gaussian EVD for M_W in head seas, this is not a surprising result. It is far more interesting to consider how well $F_{SP}(M_{SP}|M_W)_H$ and $F_{TT}(M_{TT}|M_W)_H$ from the RCWTs compare with the MCS *cdf*'s. The middle inset of Fig. 7(a) indicates that m-EDW has the best match with $F_{SP}^{\text{MCS}}(M_{SP}|M_W)_H$, the DLG has a slightly worse comparison, and m-CRRW has the worst comparison with MCS. From Fig. 6(a), it is not surprising that $F_{SP}^{\text{m-CRRW}}(M_{SP}|M_W)_H$ is the worst match to $F_{SP}^{\text{MCS}}(M_{SP}|M_W)_H$, but it is not so obvious why the m-EDW does better than the DLG for this conditional *cdf*.

Consider though, that $F_{SP}^{\text{m-EDW}}(M_{SP}|M_W)_H$ does capture the relative magnitude of $F_{SP}^{\text{MCS}}(M_{SP}|M_W)_H$, just not the fact that it is non-monotonic. Since $F_{SP}^{\text{m-EDW}}(M_{SP}|M_W)_H$ is monotonic and has a range similar to $F_{SP}^{\text{MCS}}(M_{SP}|M_W)_H$, it has more values that are within a small distance to the MCS *cdf* than does the DLG *cdf*, which is non-monotonic. But if a m-EDW conditional *cdf* does not capture the average magnitude of the respective MCS conditional *cdf*, this comparison suffers, as seen for $F_{TT}(M_{TT}|M_W)_H$ in the right inset of Fig. 7(a). In this case, both $F_{TT}^{\text{DLG}}(M_{TT}|M_W)_H$ and $F_{TT}^{\text{m-CRRW}}(M_{TT}|M_W)_H$ are a far better approximation to $F_{TT}^{\text{MCS}}(M_{TT}|M_W)_H$ than $F_{TT}^{\text{m-EDW}}(M_{TT}|M_W)_H$. Fig. 7(b) confirms that m-EDW and the DLG best match $F_{SP}^{\text{MCS}}(M_{SP}|M_W)_H$, while the DLG best matches $F_{TT}^{\text{MCS}}(M_{TT}|M_W)_H$. By construction, $F_W^{\text{m-EDW}}(M_W|M_W)_H$ and $F_W^{\text{m-CRRW}}(M_W|M_W)_H$ follow $F_W^{\text{DLG}}(M_W|M_W)_H$, as they use the same $M_W(t = 0)$ values to construct the ensemble of waves.

Figs. 8(a)–8(b) give the same comparisons for *cdf*'s conditioned on 1000-h extreme $M_{TT}(t = 0)$ responses in head seas. All $F_{TT}(M_{TT}|M_{TT})_H$ distributions match well with $F_{TT}^{\text{MCS}}(M_{TT}|M_{TT})_H$ (right inset Fig. 8(a)), again by construction. As indicated from Fig. 6(b), $F_W^{\text{m-EDW}}(M_W|M_{TT})_H$ centers on the average of $F_W^{\text{MCS}}(M_W|M_{TT})_H$, giving it a slightly better match to MCS than the DLG (left insets of Figs. 8(a)–8(b)). However, the DLG provides nearly an equally good match as m-EDW to MCS for $F_W(M_W|M_{TT})_H$ while capturing the non-monotonic nature of the conditional *cdf*, unlike m-EDW. The DLG also gives the best match to $F_{SP}^{\text{MCS}}(M_{SP}|M_{TT})_H$ as the majority of its samples are within the smallest error bound of $F_{SP}^{\text{MCS}}(M_{SP}|M_{TT})_H$ and it has the smallest point-by-point distance from $F_{SP}^{\text{MCS}}(M_{SP}|M_{TT})_H$ (middle insets of Figs. 8(a)–8(b)).

5.2. Beam seas

Fig. 9 gives the *cdf*'s from the RCWTs conditioned on 1000-h extreme $M_{LT}(t = 0)$ responses in beam seas, and confirms the conclusion from Fig. 4 that all RCWTs give a good estimate of the MCS results for this case. Figs. 10(a)–10(b) indicate that all of the RCWT conditional *cdf*'s have 100% of their values within 20% of the MCS *cdf*'s, based on each load's respective design value. In this case, m-CRRW proves the best comparison, as all $F_i^{\text{m-CRRW}}(M_I|M_{LT})_B$ have 100% of samples within 12% of the respective design value from the MCS *cdf*'s. For this case, both m-CRRW and the DLG give a better estimate to the MCS conditional *cdf*'s than m-EDW.

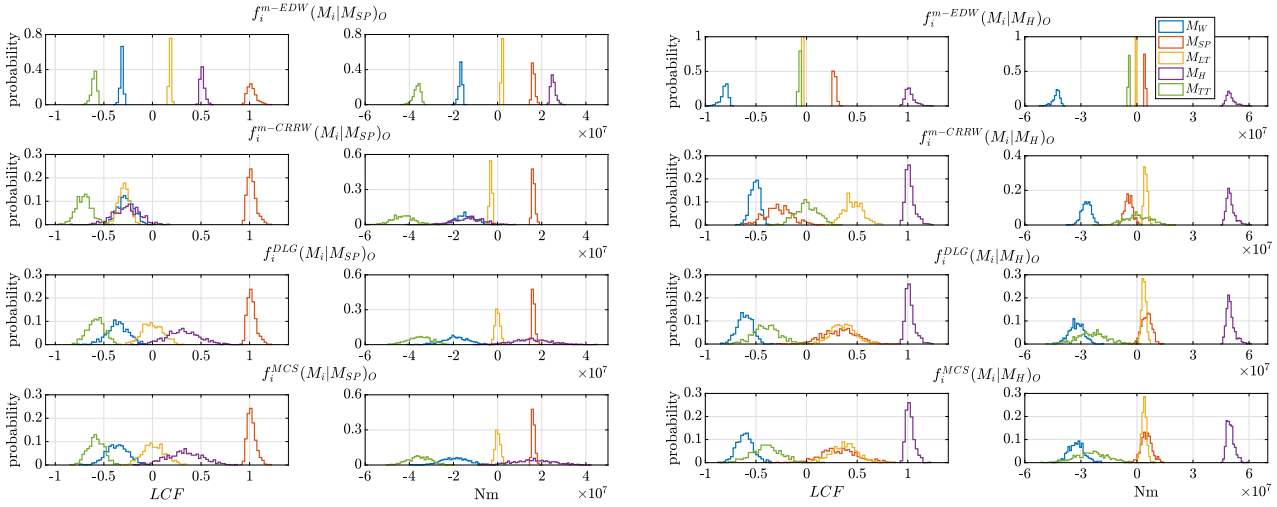

(a) $M_p = M_{SP}$ (b) $M_p = M_H$

Fig. 5. Load *pdf*'s conditioned on maximum $M_p(t=0)$ response in oblique seas (500 samples as a LCF, left column; Nm, right column).

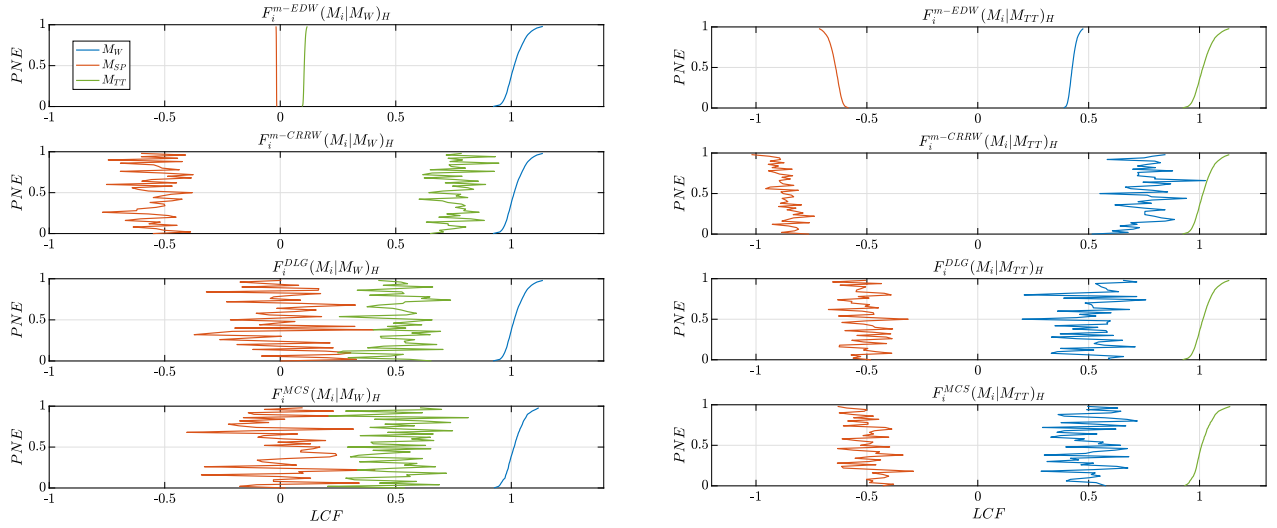

(a) $M_p = M_W$ (b) $M_p = M_{TT}$

Fig. 6. Load *cdf*'s conditioned on maximum $M_p(t=0)$ response in head seas (50 samples).

5.3. Oblique seas

Figs. 11(a)–11(b) give the *cdf*'s conditioned on 1000-h extreme $M_{SP}(t=0)$ and $M_H(t=0)$ responses in oblique seas, respectively. Figs. 12(a)–12(b) and 13(a)–13(b) give an in-depth comparison of these conditional *cdf*'s from the RCWTs with MCS. The same trends noticed from earlier cases about the performance of m-EDW, m-CRRW, and DLG in matching the MCS conditional *cdf* hold in Figs. 12(a)–12(b) and 13(a)–13(b). When the m-EDW conditional *cdf* captures the average of the MCS conditional *cdf*, it proves the best comparison (such as for $F_W(M_W|M_{SP})_O$, $F_{TT}(M_{TT}|M_{SP})_O$, and $F_{SP}(M_{SP}|M_H)_O$). But in these instances, the DLG comparison with MCS is favorable and still captures the non-monotonic nature of the MCS conditional *cdf*'s. Surprisingly, m-CRRW performs worse than m-EDW when comparing with MCS for all conditional *cdf*'s in these oblique seas cases except $F_W(M_W|M_H)_O$ and $F_{LT}(M_{LT}|M_H)_O$.

5.4. Effect of increasing primary load PNE on secondary loads

The non-monotonic nature of the MCS conditional *cdf*'s illustrates an important point about combined loading, especially relating to safety factors. That is: a primary load response associated with a higher PNE is not necessarily associated with larger simultaneous secondary loading values. In this case, a safety factor applied to the primary load may not actually lead to a load scenario which is harsher in a combined loading sense. Such a result implies that combined loading scenarios may be better defined based on a relevant limit state, versus a conditional maximum approach. The probability of not exceeding a specific load value, like primary loads which define these load scenarios, may be misleading when considering the magnitudes of the simultaneous loading conditions. It may be more relevant to examine the probability of exceeding specific combined loading scenarios which are relevant for a design limit state, as examined in Seyffert

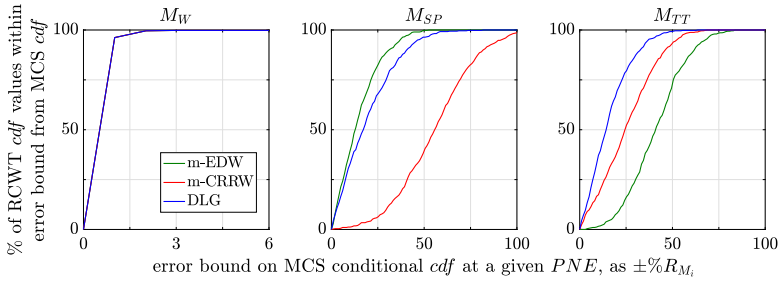

(a) Percentage of samples from RCWT conditional *cdf's* that are within a given percentage of a load design value from the corresponding MCS conditional *cdf* (considering all 500 samples).

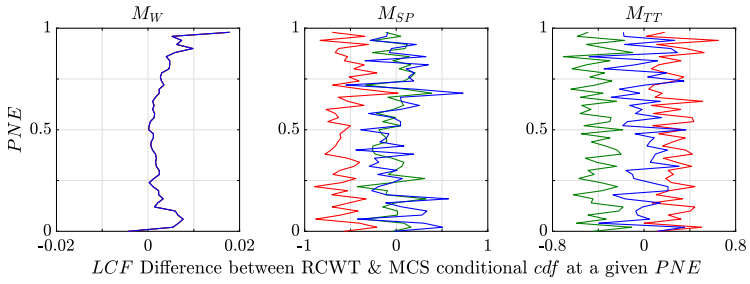

(b) *LCF* difference between RCWT and corresponding MCS conditional *cdf* (same 50 samples from Figure 6a).

Fig. 7. Comparison of RCWT & MCS *cdf*'s conditioned on maximized $M_W(t=0)$ response in head seas in a global sense (a) and in a point-by-point sense at each PNE (b).

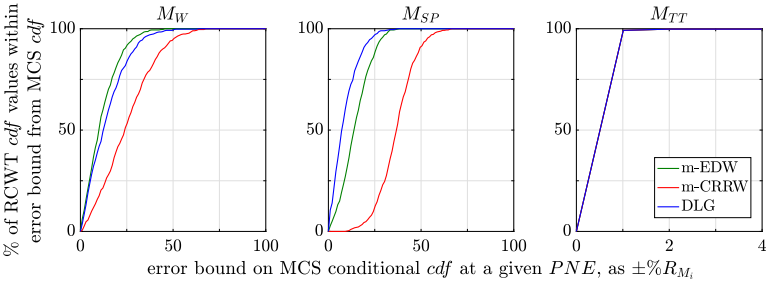

(a) Percentage of samples from RCWT conditional *cdf's* that are within a given percentage of a load design value from the corresponding MCS conditional *cdf* (considering all 500 samples).

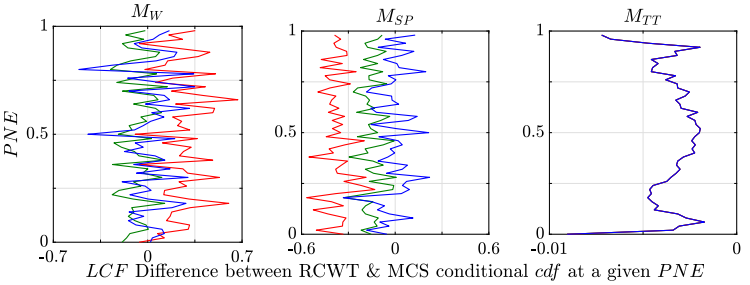

(b) *LCF* difference between RCWT and corresponding MCS conditional *cdf* (same 50 samples from Figure 6b).

Fig. 8. Comparison of RCWT & MCS *cdf*'s conditioned on maximized $M_{TT}(t=0)$ response in head seas in a global sense (a) and in a point-by-point sense at each PNE (b).

et al. (2019). In that way, a safety factor may be applied to the combined loading scenario as a whole, rather than on a primary load which defines a conditional maximum. Based on the results of this investigation, increasing the safety factor associated with a primary load for conditional maximum may not have the same effect on the secondary loads.

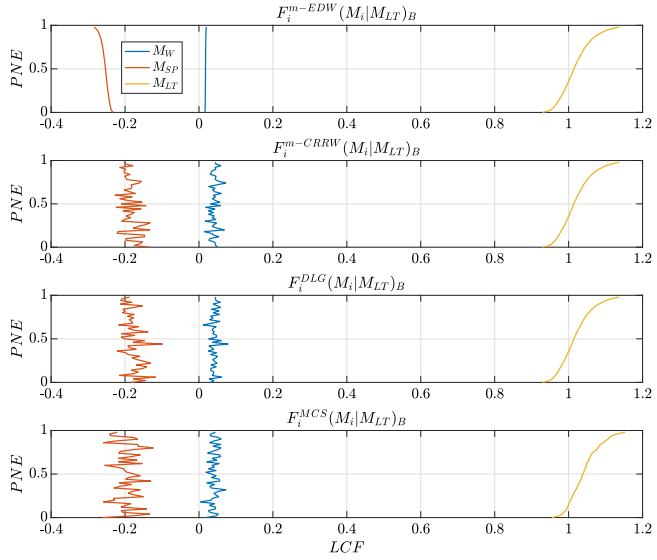

Fig. 9. Load *cdf*'s conditioned on maximum $M_{LT}(t=0)$ response in beam seas (50 samples).

6. Load vectors associated with most-likely extreme primary load response from RCWTs vs. MCS

Another interesting comparison between combined loading statistics from the RCWTs and MCS is of individual load vectors around the lifetime combined loading event at time $t = 0$. The following subsections consider these load vectors associated with the most-likely 1000-h extreme primary load response, or the response with a $PNE = 0.368$, where $M_p(t=0) = R_{M_p}$. Note that this wave for CRRW is the irregular CRRW associated with the $M_p(t=0)$ response with $PNE = 0.368$, not the MLRW. All load vector time series (from the RCWTs and MCS) have the same duration: about 22 s, centered around time $t = 0$ when the $M_p(t=0) = R_{M_p}$ response occurs.

6.1. Head seas

Fig. 14(a) shows the load combinationfactor, LCF, vector excited by the m-EDW, m-CRRW, DLG, and MCS wave that excites the $M_W(t=0)$ response in head seas with $PNE = 0.368$. The first row shows this load vector excited by m-EDW, the second row by m-CRRW, the third row by DLG, and the fourth row by MCS. The columns give different projections of this load vector. The load vector correlation matrices, Σ, are given in Eq. (A.10) in the Appendix, where the first element is M_W, the second M_{SP} and the third M_{TT}, along with the difference between the RCWT and MCS correlation matrices. Eq. (5) gives the rank and absolute value of the determinant of the difference between the RCWT and MCS correlation matrices, which quantifies the spread in the load data from the RCWTs as compared to MCS. A lower determinant indicates that the RCWT correlation matrix is more similar to the MCS correlation matrix.[2]

Load correlations for $\mathbf{M_W(t=0)}$ response with PNE = 0.368:

$$\begin{aligned} \text{rank}(\Sigma_{\text{m-EDW}}) &= 2 & |\det(\Sigma_{\text{m-EDW}} - \Sigma_{\text{MCS}})| &= 0.073 \\ \text{rank}(\Sigma_{\text{m-CRRW}}) &= 3 & |\det(\Sigma_{\text{m-CRRW}} - \Sigma_{\text{MCS}})| &= 0.134 \\ \text{rank}(\Sigma_{\text{DLG}}) &= 3 & |\det(\Sigma_{\text{DLG}} - \Sigma_{\text{MCS}})| &= 0.019 \\ \text{rank}(\Sigma_{\text{MCS}}) &= 3 \end{aligned} \quad (5)$$

A few things can be observed from comparing the load vectors excited by the different RCWT and MCS waves. The m-EDW load vector is a periodic ellipse and lies on a $2-d$ plane, unlike the m-CRRW, DLG, and MCS load vectors. This restriction of the m-EDW technique was noted in Section 2.1.1: because the m-EDW and the resulting loads are regular waves with the same frequency, the load vector is a $2-d$ ellipse. Visually, the DLG load vector seems to be the most representative of the MCS load vector.

Comparing $\Sigma_{\text{m-EDW}}$, $\Sigma_{\text{m-CRRW}}$, Σ_{DLG}, and Σ_{MCS} in Eq. (A.10) explains some of the visual differences between the RCWT and MCS-excited load vectors. Σ_{DLG} tracks the best with Σ_{MCS} in terms of the sign and relative magnitude of each correlation value, corresponding to the best visual agreement in Fig. 14(a). Comparing the determinants of the difference matrices, the DLG gives the best match to MCS, followed by m-EDW and then m-CRRW. All correlation matrices are full-rank except for $\Sigma_{\text{m-EDW}}$. Section 2.1.1 indicated that an m-EDW excited load vector has a $2-d$ range, or a correlation matrix with at maximum 2 linearly independent columns, relating to a maximum $\Sigma_{\text{m-EDW}}$ rank of 2. Due to this rank restriction of $\Sigma_{\text{m-EDW}}$, the vector of n m-EDW excited loads has a null-space dimension of $n-2$. This rank restriction of $\Sigma_{\text{m-EDW}}$ might also have consequences for constructing a joint *pdf* of these combined loads. A reasonable joint *pdf* choice could be a joint Gaussian, but since $\Sigma_{\text{m-EDW}}$ is singular, it cannot be used to assemble such a *pdf*.

Similar trends can be noticed for the load vectors excited by the m-EDW, m-CRRW, DLG, and MCS wave constructed for the $M_{TT}(t=0)$ response in head seas with $PNE = 0.368$, shown in Fig. 14(b). The load vector correlation matrices and difference between the RCWT and MCS correlation matrices are given in Eq. (A.11) in the Appendix while the rank and absolute value of the determinants of these difference matrices are given in Eq. (6). Visually the DLG-excited load vector seems to give the best agreement with the MCS load vector. In the same way, Σ_{DLG} gives best agreement to Σ_{MCS} in terms of relative magnitude and sign of the correlation terms. In both of these head seas cases, m-EDW better tracks the correlation matrix of the MCS load vector than m-CRRW.

Load correlations for $\mathbf{M_{TT}(t=0)}$ response with PNE = 0.368:

$$\begin{aligned} \text{rank}(\Sigma_{\text{m-EDW}}) &= 2 & |\det(\Sigma_{\text{m-EDW}} - \Sigma_{\text{MCS}})| &= 0.023 \\ \text{rank}(\Sigma_{\text{m-CRRW}}) &= 3 & |\det(\Sigma_{\text{m-CRRW}} - \Sigma_{\text{MCS}})| &= 0.393 \\ \text{rank}(\Sigma_{\text{DLG}}) &= 3 & |\det(\Sigma_{\text{DLG}} - \Sigma_{\text{MCS}})| &= 7.67e\text{-}5 \\ \text{rank}(\Sigma_{\text{MCS}}) &= 3 \end{aligned} \quad (6)$$

6.2. Beam seas

Fig. 15 shows the load vector normalized as a LCF which is excited by the m-EDW, m-CRRW, DLG, and MCS wave that excites the $M_{LT}(t=0)$ response in beam seas with $PNE = 0.368$. The load vector correlation matrices and the difference between the RCWT and MCS correlation matrices are given in Eq. (A.12) in the Appendix, where order of the elements is M_W, M_{SP} and M_{LT}. The ranks of the correlation matrices and absolute value of the determinant of the difference matrices are given in Eq. (7). Comparing the determinants of the difference matrices in Eq. (7), the DLG best captures the MCS load correlations for this case, followed by m-CRRW and then m-EDW.

[2] The difference $\Sigma_{RCWT} - \Sigma_{MCS}$ and the absolute value of $\det(\Sigma_{RCWT} - \Sigma_{MCS})$ can be interpreted similarly as evaluating the spread of data around its mean. The difference $\Sigma_{RCWT} - \Sigma_{MCS}$ shows how similar the RCWT and MCS correlation values are. The value $|\det(\Sigma_{RCWT} - \Sigma_{MCS})|$ captures the volume of the data cloud associated with the RCWT correlation values centered around the MCS correlation values. The determinant of an N by N matrix is equal to the product of the matrix eigenvalues; those eigenvalues correspond to the variance along the principal axis components of the matrix data. The product of these eigenvalues, or the matrix determinant, quantifies the hyper-volume whose edges are defined by the matrix vectors. If $\Sigma_{RCWT} = \Sigma_{MCS}$, the volume of the resulting data cloud centered around the MCS mean would be exactly zero.

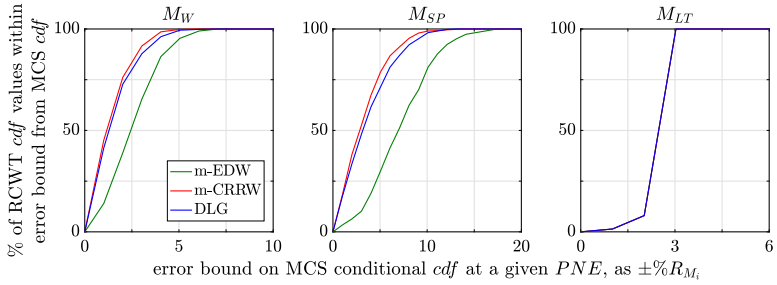

(a) Percentage of samples from RCWT conditional *cdf's* that are within a given percentage of a load design value from the corresponding MCS conditional *cdf* (considering all 500 samples).

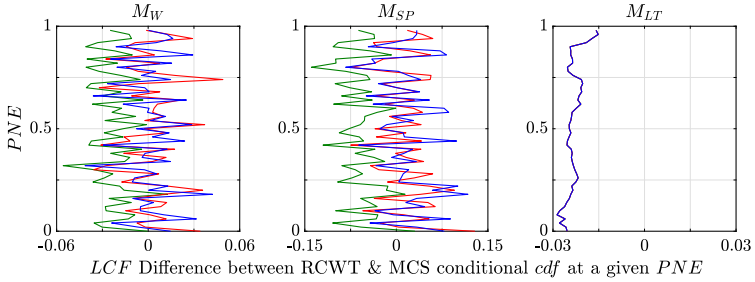

(b) *LCF* difference between RCWT and corresponding MCS conditional *cdf* (same 50 samples from Figure 9).

Fig. 10. Comparison of RCWT & MCS *cdf*'s conditioned on maximized $M_{LT}(t=0)$ response in beam seas in a global sense (a) and in a point-by-point sense at each PNE (b).

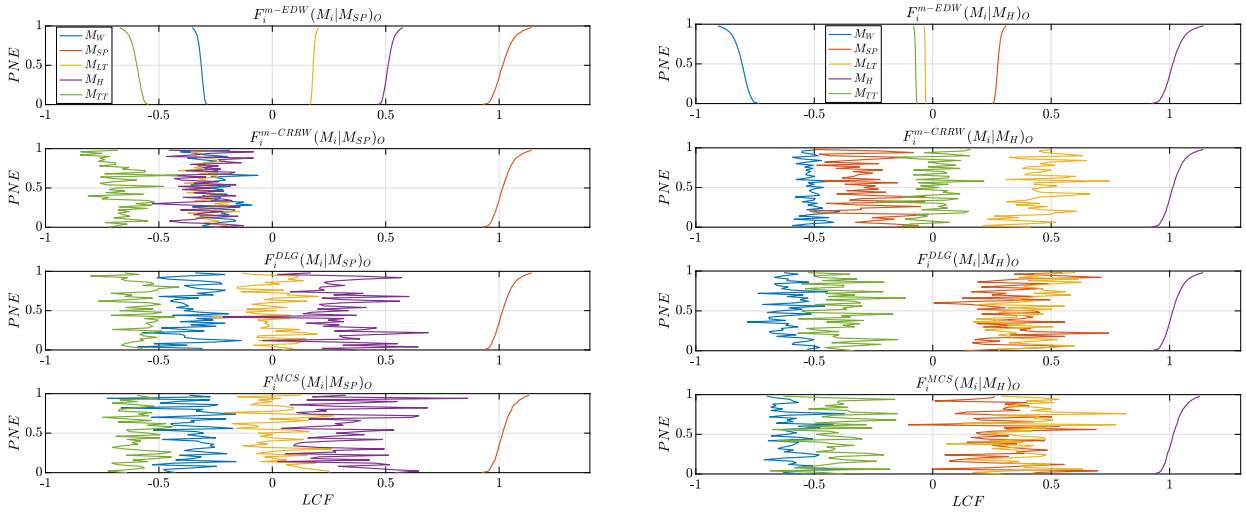

(a) $M_p = M_{SP}$ (b) $M_p = M_H$

Fig. 11. Load *cdf*'s conditioned on maximum $M_p(t=0)$ response in oblique seas (50 samples).

Load correlations for $M_{LT}(t=0)$ response with PNE = 0.368 :

$$\begin{aligned}
\text{rank}(\Sigma_{\text{m-EDW}}) &= 2\\
\text{rank}(\Sigma_{\text{m-CRRW}}) &= 3\\
\text{rank}(\Sigma_{\text{DLG}}) &= 3\\
\text{rank}(\Sigma_{\text{MCS}}) &= 3\\
|\det(\Sigma_{\text{m-EDW}} - \Sigma_{\text{MCS}})| &= 0.050\\
|\det(\Sigma_{\text{m-CRRW}} - \Sigma_{\text{MCS}})| &= 0.003\\
|\det(\Sigma_{\text{DLG}} - \Sigma_{\text{MCS}})| &= 5.31e\text{-}6
\end{aligned} \tag{7}$$

6.3. Oblique seas

Fig. 16 shows the load vector normalized as a LCF which is excited by the m-EDW, m-CRRW, DLG, and MCS wave that excites the 1000-h extreme $M_{SP}(t=0)$ response in oblique seas with $PNE = 0.368$. The oblique seas condition considers all 5 global loads so only the $2-d$ projections of this vector are plotted. The load vector correlation matrices and the $\Sigma_{RCWT} - \Sigma_{MCS}$ matrices are given in Eq. (A.13) in the Appendix where order of the elements is M_W, M_{SP}, M_{LT}, M_H, and M_{TT}. Eq. (8) gives the ranks and absolute values of the determinants of

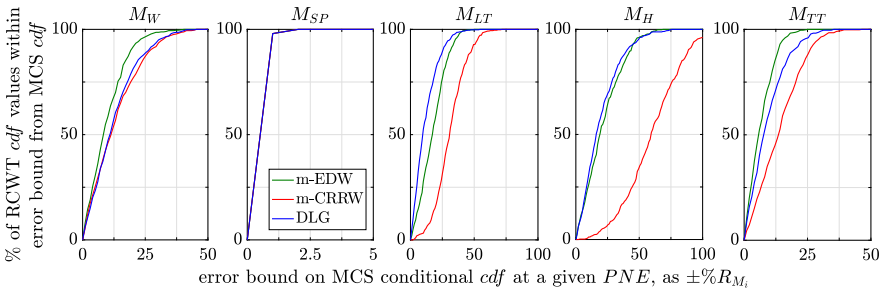

(a) Percentage of samples from RCWT conditional *cdf*'s that are within a given percentage of a load design value from the corresponding MCS conditional *cdf* (considering all 500 samples).

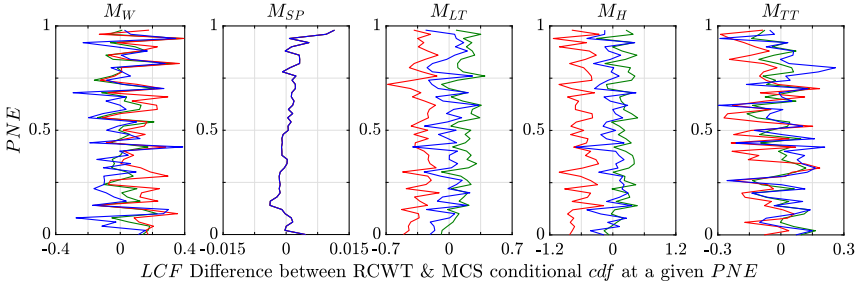

(b) *LCF* difference between RCWT and corresponding MCS conditional *cdf* (same 50 samples from Figure 11a).

Fig. 12. Comparison of RCWT & MCS *cdf*'s conditioned on maximized $M_{SP}(t=0)$ response in oblique seas in a global sense (a) and in a point-by-point sense at each PNE (b).

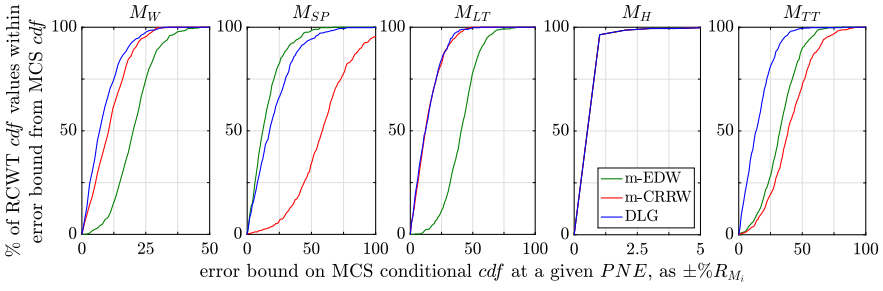

(a) Percentage of samples from RCWT conditional *cdf*'s that are within a given percentage of a load design value from the corresponding MCS conditional *cdf* (considering all 500 samples).

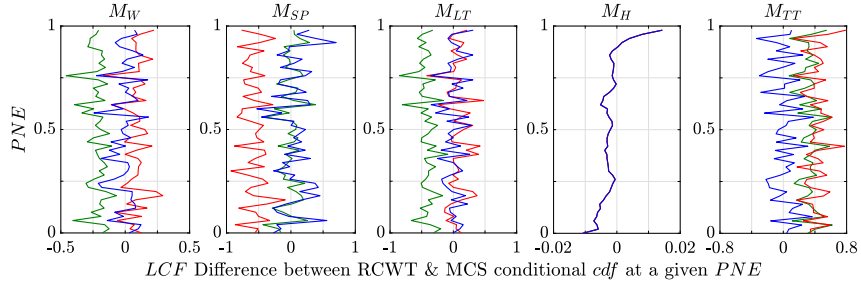

(b) *LCF* difference between RCWT and corresponding MCS conditional *cdf* (same 50 samples from Figure 11b).

Fig. 13. Comparison of RCWT & MCS *cdf*'s conditioned on maximized $M_H(t=0)$ response in oblique seas in a global sense (a) and in a point-by-point sense at each PNE (b).

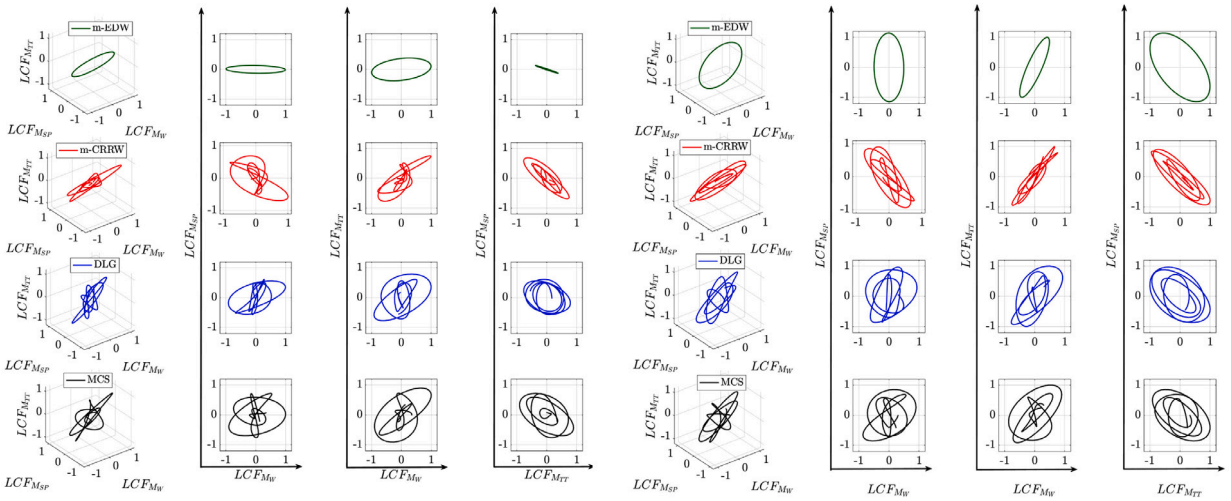

(a) $M_p = M_W$ (b) $M_p = M_{TT}$

Fig. 14. Loads excited by m-EDW, m-CRRW, DLG, & MCS wave leading to head seas $M_p(t=0)$ response with $PNE = 0.368$.

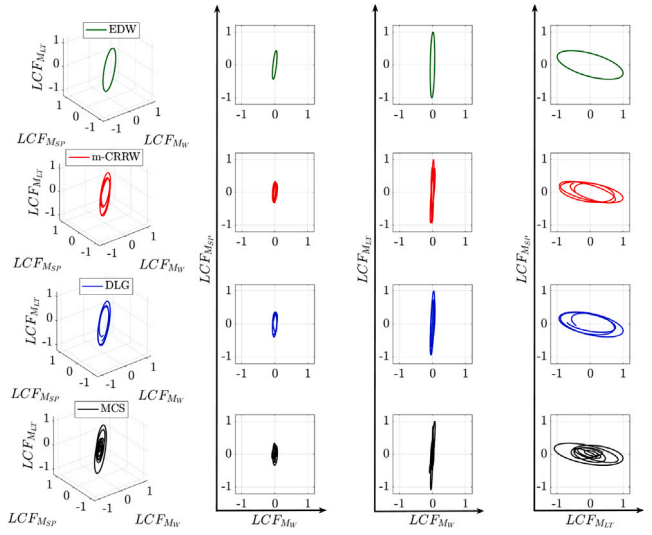

Fig. 15. Loads excited by m-EDW, m-CRRW, DLG, & MCS wave leading to beam seas $M_{LT}(t=0)$ response with $PNE = 0.368$. The ranks of the covariance matrices and the absolute value of the determinant of each $\Sigma_{RCWT} - \Sigma_{MCS}$ matrix are given.

the difference matrices for this load case based on $M_{SP}(t=0) = R_{M_{SP}}$.

Load correlations for $M_{SP}(t=0)$ response with PNE = 0.368:

$$\begin{aligned} \text{rank}(\Sigma_{\text{m-EDW}}) &= 2 & |\det(\Sigma_{\text{m-EDW}} - \Sigma_{\text{MCS}})| &= 4.78e\text{-}5 \\ \text{rank}(\Sigma_{\text{m-CRRW}}) &= 5 & |\det(\Sigma_{\text{m-CRRW}} - \Sigma_{\text{MCS}})| &= 0.010 \\ \text{rank}(\Sigma_{\text{DLG}}) &= 5 & |\det(\Sigma_{\text{DLG}} - \Sigma_{\text{MCS}})| &= 2.93e\text{-}7 \\ \text{rank}(\Sigma_{\text{MCS}}) &= 5 \end{aligned} \tag{8}$$

In the oblique seas case, the range limitation of the m-EDW excited load vector is more apparent, as the load vector still lies on a $2-d$ plane in the $5-d$ space. This is reflected by $\Sigma_{\text{m-EDW}}$, which still has rank 2, even though this case includes all 5 global loads. Despite this limitation, m-EDW still tracks the MCS load correlations quite well. But overall, the DLG has the best load correlation match with MCS for this case, supported by the remarkable visual comparison between the MCS and DLG wave leading to the $M_{SP}(t=0)$ response with $PNE = 0.368$. The DLG wave excites very similar load vector shape patterns as MCS, especially in the $LCF_{M_W} - LCF_{M_{LT}}$, $LCF_{M_{SP}} - LCF_{M_{LT}}$, $LCF_{M_{SP}} - LCF_{M_H}$, and $LCF_{M_{LT}} - LCF_{M_H}$ planes (2nd, 5th, 6th, and 8th columns). Considering the comparison is of load vectors excited by single irregular waves, rather than an ensemble average wave, it is impressive that the DLG recovers such a similar simultaneous loading response.

Although the m-EDW excited load vector corresponding to the $M_{SP}(t=0)$ response in oblique seas with $PNE = 0.368$ does not visually track as well with the MCS load vector in terms of the details of the load vector shape, it still gives a favorable estimation of the load correlations. Similar to the comparisons of the conditional *cdf*'s, although the m-EDW wave does not capture the details (e.g., the non-monotonic nature of the *cdf*'s or the randomness of the load vector), it does globally describe the combined loading scenario when considering the load correlations. m-CRRW *does* lead to an irregular load vector like MCS, but does not estimate these load correlations as well as m-EDW.

Fig. 17 shows the load vectors excited by the RCWTs and MCS associated with the $M_H(t=0)$ response in oblique seas with $PNE = 0.368$. The load correlation matrices, difference matrices, ranks of the correlation matrices, and determinants of the difference matrices are given in Eq. (A.14) and Eq. (9), respectively. Again in this case, the DLG proves the best visual match to the MCS load vectors, especially in the $LCF_{M_W} - LCF_{M_{LT}}$, $LCF_{M_W} - LCF_{M_H}$, and $LCF_{M_{LT}} - LCF_{M_H}$ planes (2nd, 3rd, and 8th columns). Based on the determinant of the difference matrices in Eq. (9), the DLG by far best matches the MCS load correlations.

Load correlations for $M_H(t=0)$ response with PNE = 0.368:

$$\begin{aligned} \text{rank}(\Sigma_{\text{m-EDW}}) &= 2 & |\det(\Sigma_{\text{m-EDW}} - \Sigma_{\text{MCS}})| &= 0.023 \\ \text{rank}(\Sigma_{\text{m-CRRW}}) &= 5 & |\det(\Sigma_{\text{m-CRRW}} - \Sigma_{\text{MCS}})| &= 0.001 \\ \text{rank}(\Sigma_{\text{DLG}}) &= 5 & |\det(\Sigma_{\text{DLG}} - \Sigma_{\text{MCS}})| &= 2.68e\text{-}6 \\ \text{rank}(\Sigma_{\text{MCS}}) &= 5 \end{aligned} \tag{9}$$

7. Computational effort associated with RCWTs vs. MCS

The final comparison to distinguish the RCWTs is the computational effort associated with constructing the lifetime combined loading scenarios. Mainly, does a RCWT give up accuracy at the expense of efficiency, or vice-versa? Table 3 tabulates the computational effort associated with generating the 500 wave profiles via the RCWTs and MCS

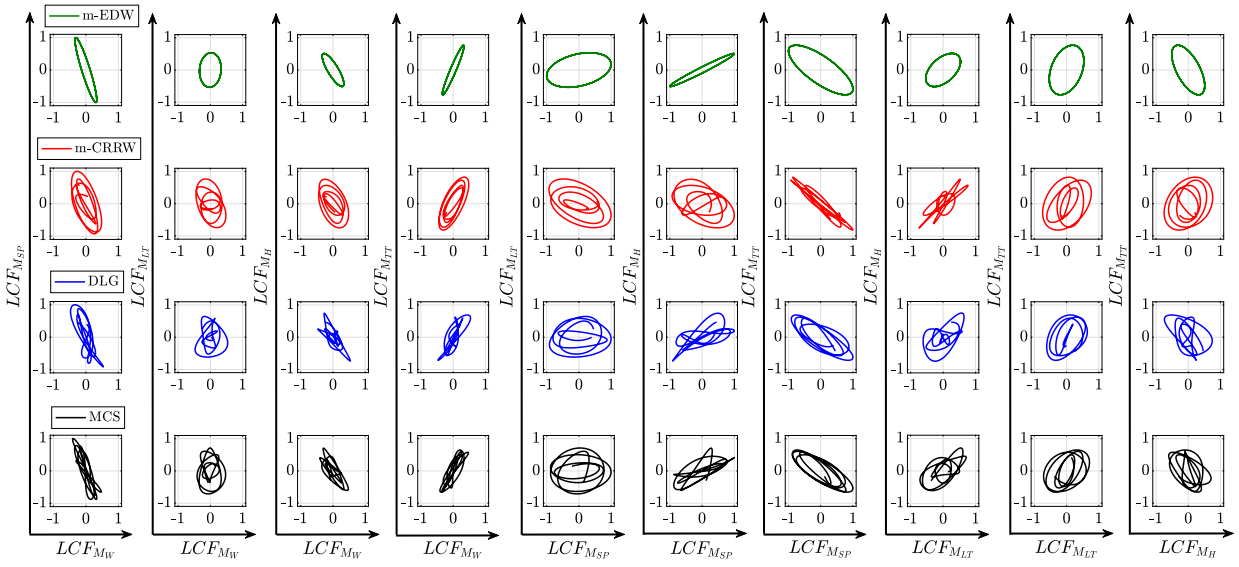

Fig. 16. Loads excited by EDW, CRRW, DLG, & MCS wave leading to oblique seas $M_{SP}(t=0)$ response with $PNE = 0.368$.

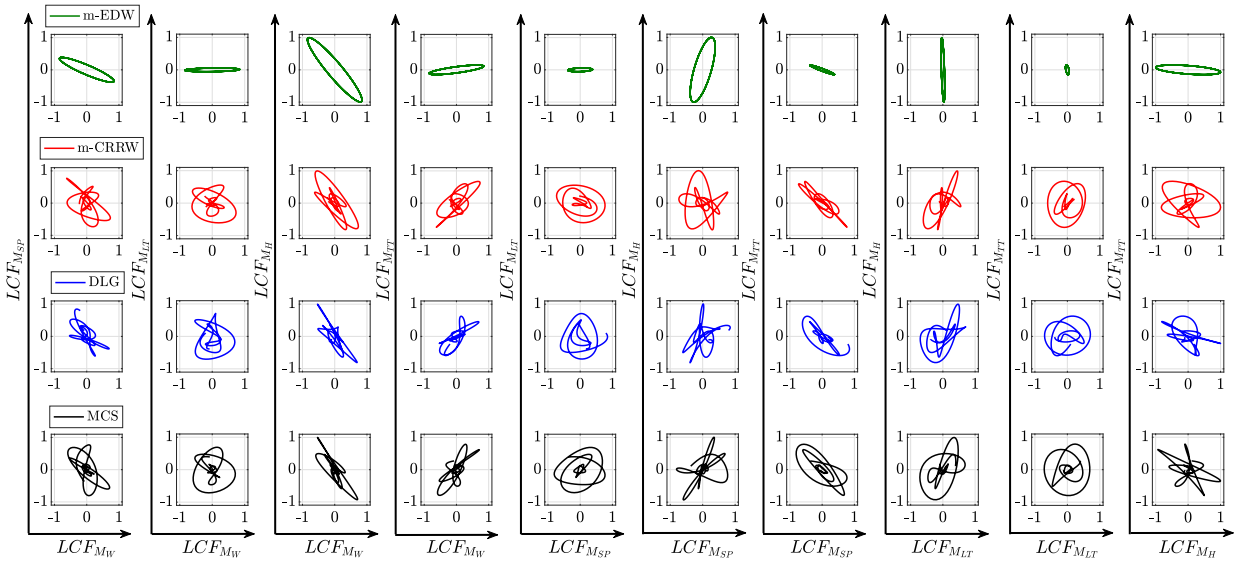

Fig. 17. Loads excited by EDW, CRRW, DLG, & MCS wave leading to oblique seas $M_H(t=0)$ response with $PNE = 0.368$.

and collecting the conditional maxima statistics for the 5 combined loading scenarios investigated in this paper. The m-EDW, m-CRRW, and DLG waves and load statistics were generated via a MacBook Pro 2.3 GHs Intel Core i5. The MCS were run on an Ubuntu desktop with 12x Intel(R) Xeon(R) CPU E5-2609 v3 @ 1.90 GHz. The difference in computational effort between m-EDW and m-CRRW is essentially negligible for engineering purposes. Although the DLG takes longer, it is still efficient compared to MCS.

Table 3
Computation time to generate wave profiles and collect combined loading statistics for RCWTs vs. MCS.

Method	Computation time
m-EDW	<1 s
m-CRRW	≈1.5 s
DLG	≈3 min
MCS	≈8 h

8. Discussion of RCWT performance

Section 3.3 introduced four points of comparison to evaluate the RCWTs. This section summarizes the results from Section 4 - Section 7 to give an overall comparison of the different RCWT performances as compared to MCS.

8.1. RCWT leading to best pdf match

Examining the combined load conditional *pdf*'s from the RCWTs with MCS in Section 4, the DLG gives the best visual comparison with

MCS, in terms of load magnitude and variance, for all cases except beam seas, where DLG and m-CRRW seem to give equally good comparisons. Comparing just m-CRRW and m-EDW, m-CRRW much better captures the load variance than m-EDW. But both the m-EDW and m-CRRW technique can far over or under-estimate a load magnitude as compared to MCS, which could be problematic if these load cases are used as inputs to high-fidelity structural models to test structural compliance with classification society criteria.

Examining the conditional *pdf*'s also indicates that there may be significant variability in short-term extreme combined loading responses. It may not be possible to accurately describe short-term extreme combined loading scenarios by a single LCF combination, which would not describe the potential load variability within that load case. Rather, a distribution of extreme combined loading responses may need to be considered.

8.2. RCWT leading to best cdf match

Comparing the conditional load *cdf*'s from the RCWTs with MCS in Section 5, the DLG gives either the best, or a close second best, comparison with the MCS for all $F_i(M_i|M_p)$ where $M_i \neq M_p$. The DLG captures the non-monotonic nature of the MCS conditional *cdf*'s with relatively low error. In fact, the DLG best matches the MCS conditional *cdf*'s in 7/14 cases, only considering $F_i(M_i|M_p)$ where $M_i \neq M_p$. In 5/14 of these conditional *cdf*'s, the EDW proves the best match but the DLG comes in a close second. Surprisingly, m-CRRW only gives the best match with MCS for the two beam seas cases where $M_i \neq M_p$.

Comparing just the m-CRRW and m-EDW conditional *cdf*'s $F_i(M_i|M_p)$ where $M_i \neq M_p$, m-CRRW only out-performs m-EDW in 5 cases: $F_{TT}(M_{TT}|M_W)_H$, $F_W(M_W|M_{LT})_B$, $F_{SP}(M_{SP}|M_{LT})_B$, $F_W(M_W|M_H)_O$, and $F_{LT}(M_{LT}|M_H)_O$. But a visual inspection of these *cdf*'s in Figs. 5 (Fig. 6(a), 9, and 11(b)) indicates that for the cases when m-CRRW outperforms m-EDW, only in three cases ($F_W(M_W|M_{LT})_B$, $F_{SP}(M_{SP}|M_{LT})_B$, and $F_{LT}(M_{LT}|M_H)_O$) does m-CRRW give a *good* approximation to MCS. For the other two cases ($F_{TT}(M_{TT}|M_W)_H$ and $F_W(M_W|M_H)_O$) the comparison of m-CRRW to MCS is better than m-EDW to MCS, but m-CRRW still does not give an accurate representation of the respective MCS *cdf*'s in terms of load magnitude. The m-CRRW technique does capture the non-monotonic nature of the MCS conditional *cdf*'s, but does not reliably capture the MCS load magnitude for every load scenario.

8.3. RCWT leading to best load correlation match

Examining the load vectors associated with the most-likely 1000-h extreme $M_p(t = 0)$ responses in Section 6 again suggests DLG gives the best comparison with MCS. The DLG waves exciting the 1000-h most-likely extreme $M_p(t = 0)$ responses led to the closest load correlation comparison to MCS for all of the examined cases. The DLG waves also led to very similar load vector shapes as the associated MCS waves, even though this comparison was of single stochastic simulations and not ensemble averages. Comparing just m-CRRW and m-EDW, m-CRRW only out-performs m-EDW for the load vectors based on extreme $M_{LT}(t = 0)$ response in beam seas and extreme $M_H(t = 0)$ response in oblique seas. On the other hand, m-EDW out-performs m-CRRW for matching the equivalent MCS load correlations extreme $M_W(t = 0)$ and $M_{TT}(t = 0)$ in head seas and extreme $M_{SP}(t = 0)$ in oblique seas, even though the m-EDW correlation matrices are rank-deficient.

8.4. Efficient vs. realistic

Clearly the m-EDW and m-CRRW are the most efficient RCWTs, although the computation time for the DLG is still minimal when compared to brute-force MCS and for engineering purposes. Considering that the m-EDW and m-CRRW methods are based on a similar idea (i.e. Airy wave theory, or phase-shifting frequency components to lead to maximum load responses), the added computation time to include all wave frequencies (m-CRRW) versus using a single wave frequency (m-EDW) is negligible. But based on the combined loading statistics evaluated for this trimaran hull, it is not clear that using the m-CRRW technique results in more realistic extreme combined loading scenarios than does the m-EDW technique, as compared to MCS.

Waves from the m-CRRW technique are certainly more physically realistic because they are irregular. But the waves from the m-CRRW technique did not reliably excite more realistic combined loading scenarios for the examined trimaran hull than the waves from the m-EDW technique. Surprisingly, the combined loading scenarios from the m-EDW technique seem to better represent the MCS load scenarios than m-CRRW, despite the fact that the m-EDW is truly a simplification of the m-CRRW technique. At the very least, m-CRRW did not present a significant improvement over m-EDW when defining extreme combined loading scenarios for this trimaran hull.

9. Conclusions

This paper investigated 1000-h extreme combined loading statistics on a trimaran generated by three response-conditioning wave techniques: a modified Equivalent Design Wave (m-EDW) approach, modified Conditioned Random Response Wave (m-CRRW) approach, and the Design Loads Generator (DLG), and compared the results with load statistics from brute-force Monte Carlo Simulations (MCS).

This investigation illustrated m-EDW and m-CRRW approaches which construct ensembles of waves that lead to a distribution of extreme loading responses. It is at least recommended to use these m-EDW and m-CRRW techniques instead of the traditional EDW and CRRW techniques to account for the possible extreme load variability of short-term combined loading scenarios, as the variance in the simultaneous loading distributions can be substantial. Compared to the analyses in Seyffert and Kana (2019) and Seyffert et al. (2018), the m-EDW technique represents a major improvement over using a single EDW to describe combined loading scenarios on this trimaran hull. Comparing just m-EDW and m-CRRW, it is not clear if m-CRRW offers any significant advantage over m-EDW in realistically describing extreme combined loading scenarios for the examined trimaran hull.

Overall, the DLG provides the best comparison with MCS when describing extreme combined loading scenarios for this trimaran, with a significant reduction in computation time. The DLG captured the load magnitude and variance of the conditional extreme loading *pdf*'s, the non-monotonic nature of the conditional *cdf*'s, and the irregular loading profiles and resulting load correlations for a specific risk parameter (i.e. extreme primary load response with $PNE = 0.368$). This investigation confirms the suitability of the DLG, based on efficiency and comparisons with brute-force stochastic simulations, to construct wave environments leading to rare return-period responses, even for rare combined loading scenarios on a complex hull like a trimaran.

Acknowledgments

The authors would like to thank Ms. Kelly Cooper and the Office of Naval Research for their support for this research which is funded under the Naval International Cooperative Opportunities in Science and Technology Program (NICOP) contract number N00014-15-1-2752.

Appendix

Loads Conditioned on extreme $M_W(t = 0)$ response in head seas with PNE = 0.368:

$$\Sigma_{\text{m-EDW}} = \begin{bmatrix} 1 & -0.12 & 0.26 \\ -0.12 & 1 & -0.99 \\ 0.26 & -0.99 & 1 \end{bmatrix} \quad \text{rank}(\Sigma_{\text{m-EDW}}) = 2 \quad \Sigma_{\text{m-EDW}} - \Sigma_{\text{MCS}} = \begin{bmatrix} 0 & -0.27 & -0.25 \\ -0.27 & 0 & -0.54 \\ -0.25 & -0.54 & 0 \end{bmatrix} \quad |\det(\Sigma_{\text{m-EDW}} - \Sigma_{\text{MCS}})| = 0.073 \tag{A.10}$$

$$\Sigma_{\text{m-CRRW}} = \begin{bmatrix} 1 & -0.56 & 0.74 \\ -0.56 & 1 & -0.87 \\ 0.74 & -0.87 & 1 \end{bmatrix} \quad \text{rank}(\Sigma_{\text{m-CRRW}}) = 3 \quad \Sigma_{\text{m-CRRW}} - \Sigma_{\text{MCS}} = \begin{bmatrix} 0 & -0.71 & 0.22 \\ -0.71 & 0 & -0.42 \\ 0.22 & -0.42 & 0 \end{bmatrix} \quad |\det(\Sigma_{\text{m-CRRW}} - \Sigma_{\text{MCS}})| = 0.134$$

$$\Sigma_{\text{DLG}} = \begin{bmatrix} 1 & 0.51 & 0.38 \\ 0.51 & 1 & -0.25 \\ 0.38 & -0.25 & 1 \end{bmatrix} \quad \text{rank}(\Sigma_{\text{DLG}}) = 3 \quad \Sigma_{\text{DLG}} - \Sigma_{\text{MCS}} = \begin{bmatrix} 0 & 0.37 & -0.13 \\ 0.37 & 0 & 0.19 \\ -0.13 & 0.19 & 0 \end{bmatrix} \quad |\det(\Sigma_{\text{DLG}} - \Sigma_{\text{MCS}})| = 0.019$$

$$\Sigma_{\text{MCS}} = \begin{bmatrix} 1 & 0.15 & 0.51 \\ 0.15 & 1 & -0.45 \\ 0.51 & -0.45 & 1 \end{bmatrix} \quad \text{rank}(\Sigma_{\text{MCS}}) = 3$$

Loads Conditioned on extreme $M_{TT}(t = 0)$ response in head seas with PNE = 0.368:

$$\Sigma_{\text{m-EDW}} = \begin{bmatrix} 1 & -0.05 & 0.85 \\ -0.05 & 1 & -0.56 \\ 0.85 & -0.56 & 1 \end{bmatrix} \quad \text{rank}(\Sigma_{\text{m-EDW}}) = 2 \quad \Sigma_{\text{m-EDW}} - \Sigma_{\text{MCS}} = \begin{bmatrix} 0 & -0.26 & 0.36 \\ -0.26 & 0 & -0.13 \\ 0.36 & -0.13 & 0 \end{bmatrix} \quad |\det(\Sigma_{\text{m-EDW}} - \Sigma_{\text{MCS}})| = 0.023 \tag{A.11}$$

$$\Sigma_{\text{m-CRRW}} = \begin{bmatrix} 1 & -0.79 & 0.93 \\ -0.79 & 1 & -0.89 \\ 0.93 & -0.89 & 1 \end{bmatrix} \quad \text{rank}(\Sigma_{\text{m-CRRW}}) = 3 \quad \Sigma_{\text{m-CRRW}} - \Sigma_{\text{MCS}} = \begin{bmatrix} 0 & -1.00 & 0.44 \\ -1.00 & 0 & -0.45 \\ 0.44 & -0.45 & 0 \end{bmatrix} \quad |\det(\Sigma_{\text{m-CRRW}} - \Sigma_{\text{MCS}})| = 0.393$$

$$\Sigma_{\text{DLG}} = \begin{bmatrix} 1 & 0.24 & 0.58 \\ 024 & 1 & -0.45 \\ 0.58 & -0.45 & 1 \end{bmatrix} \quad \text{rank}(\Sigma_{\text{DLG}}) = 3 \quad \Sigma_{\text{DLG}} - \Sigma_{\text{MCS}} = \begin{bmatrix} 0 & -0.03 & 0.09 \\ -0.03 & 0 & -0.02 \\ 0.09 & -0.02 & 0 \end{bmatrix} \quad |\det(\Sigma_{\text{DLG}} - \Sigma_{\text{MCS}})| = 7.67e\text{-}5$$

$$\Sigma_{\text{MCS}} = \begin{bmatrix} 1 & 0.21 & 0.50 \\ 0.21 & 1 & -0.44 \\ 0.50 & -0.44 & 1 \end{bmatrix} \quad \text{rank}(\Sigma_{\text{MCS}}) = 3$$

Loads Conditioned on extreme $M_{LT}(t = 0)$ response in beam seas with PNE = 0.368:

$$\Sigma_{\text{m-EDW}} = \begin{bmatrix} 1 & 0.63 & 0.26 \\ 0.63 & 1 & -0.59 \\ 0.26 & -0.59 & 1 \end{bmatrix} \quad \text{rank}(\Sigma_{\text{m-EDW}}) = 2 \quad \Sigma_{\text{m-EDW}} - \Sigma_{\text{MCS}} = \begin{bmatrix} 0 & 0.42 & -0.40 \\ 0.42 & 0 & -0.15 \\ -0.40 & -0.15 & 0 \end{bmatrix} \quad |\det(\Sigma_{\text{m-EDW}} - \Sigma_{\text{MCS}})| = 0.050 \tag{A.12}$$

$$\Sigma_{\text{m-CRRW}} = \begin{bmatrix} 1 & 0.35 & 0.54 \\ 0.35 & 1 & -0.52 \\ 0.54 & -0.52 & 1 \end{bmatrix} \quad \text{rank}(\Sigma_{\text{m-CRRW}}) = 3 \quad \Sigma_{\text{m-CRRW}} - \Sigma_{\text{MCS}} = \begin{bmatrix} 0 & 0.14 & -0.12 \\ 0.14 & 0 & -0.08 \\ -0.12 & -0.08 & 0 \end{bmatrix} \quad |\det(\Sigma_{\text{m-CRRW}} - \Sigma_{\text{MCS}})| = 0.003$$

$$\Sigma_{\text{DLG}} = \begin{bmatrix} 1 & 0.28 & 0.71 \\ 0.28 & 1 & -0.44 \\ 0.71 & -0.44 & 1 \end{bmatrix} \quad \text{rank}(\Sigma_{\text{DLG}}) = 3 \quad \Sigma_{\text{DLG}} - \Sigma_{\text{MCS}} = \begin{bmatrix} 0 & 0.07 & 0.05 \\ 0.07 & 0 & 0.001 \\ 0.05 & 0.001 & 0 \end{bmatrix} \quad |\det(\Sigma_{\text{DLG}} - \Sigma_{\text{MCS}})| = 5.31e\text{-}6$$

$$\Sigma_{\text{MCS}} = \begin{bmatrix} 1 & 0.21 & 0.66 \\ 0.21 & 1 & -0.44 \\ 0.66 & -0.44 & 1 \end{bmatrix} \quad \text{rank}(\Sigma_{\text{MCS}}) = 3$$

Loads Conditioned on extreme $M_{SP}(t = 0)$ response in oblique seas with PNE = 0.368:

$$\Sigma_{\text{m-EDW}} = \begin{bmatrix} 1 & -0.92 & 0.06 & -0.83 & 0.96 \\ -0.92 & 1 & 0.33 & 0.98 & -0.77 \\ 0.06 & 0.33 & 1 & 0.50 & 0.35 \\ -0.83 & 0.98 & 0.50 & 1 & -0.63 \\ 0.96 & -0.77 & 0.35 & -0.63 & 1 \end{bmatrix} \quad \text{rank}(\Sigma_{\text{m-EDW}}) = 2 \quad \Sigma_{\text{m-EDW}} - \Sigma_{\text{MCS}} = \begin{bmatrix} 0 & -0.06 & 0.03 & -0.05 & 0.09 \\ -0.06 & 0 & 0.27 & 0.25 & 0.04 \\ 0.03 & 0.27 & 0 & -0.07 & -0.05 \\ -0.05 & 0.25 & -0.07 & 0 & -0.17 \\ 0.09 & 0.04 & -0.05 & -0.17 & 0 \end{bmatrix} \tag{A.13}$$

$$\Sigma_{\text{m-CRRW}} = \begin{bmatrix} 1 & -0.65 & -0.29 & -0.51 & 0.74 \\ -0.65 & 1 & -0.46 & -0.28 & -0.96 \\ -0.29 & -0.46 & 1 & 0.82 & 0.35 \\ -0.51 & -0.28 & 0.82 & 1 & 0.18 \\ 0.74 & -0.96 & 0.35 & 0.18 & 1 \end{bmatrix} \quad \text{rank}(\Sigma_{\text{m-CRRW}}) = 5 \quad \Sigma_{\text{m-CRRW}} - \Sigma_{\text{MCS}} = \begin{bmatrix} 0 & 0.20 & -0.33 & 0.27 & -0.12 \\ 0.20 & 0 & -0.52 & -1.01 & -0.16 \\ -0.33 & -0.52 & 0 & 0.25 & -0.05 \\ 0.27 & -1.01 & 0.25 & 0 & 0.65 \\ -0.12 & -0.16 & -0.05 & 0.65 & 0 \end{bmatrix}$$

$$\Sigma_{\text{DLG}} = \begin{bmatrix} 1 & -0.76 & 0.07 & -0.76 & 0.80 \\ -0.76 & 1 & 0.09 & 0.65 & -0.77 \\ 0.07 & 0.09 & 1 & 0.54 & 0.41 \\ -0.76 & 0.65 & 0.54 & 1 & -0.43 \\ 0.80 & -0.77 & 0.41 & -0.43 & 1 \end{bmatrix} \quad \text{rank}(\Sigma_{\text{DLG}}) = 5 \quad \Sigma_{\text{DLG}} - \Sigma_{\text{MCS}} = \begin{bmatrix} 0 & 0.10 & 0.04 & 0.02 & -0.07 \\ 0.10 & 0 & 0.03 & -0.08 & 0.03 \\ 0.04 & 0.03 & 0 & -0.04 & 0.01 \\ 0.02 & -0.08 & -0.04 & 0 & 0.04 \\ -0.07 & 0.03 & 0.01 & 0.04 & 0 \end{bmatrix}$$

$$\Sigma_{\text{MCS}} = \begin{bmatrix} 1 & -0.86 & 0.03 & -0.78 & 0.86 \\ -0.86 & 1 & 0.06 & 0.73 & -0.80 \\ 0.03 & 0.06 & 1 & 0.57 & 0.40 \\ -0.78 & 0.73 & 0.57 & 1 & -0.47 \\ 0.86 & -0.80 & 0.40 & -0.47 & 1 \end{bmatrix} \quad \text{rank}(\Sigma_{\text{MCS}}) = 5 \quad \begin{array}{c} |\det(\Sigma_{\text{m-EDW}} - \Sigma_{\text{MCS}})| = 4.78e\text{-}5 \\ |\det(\Sigma_{\text{m-CRRW}} - \Sigma_{\text{MCS}})| = 0.010 \\ |\det(\Sigma_{\text{DLG}} - \Sigma_{\text{MCS}})| = 2.93e\text{-}7 \end{array}$$

Loads Conditioned on extreme $M_H(t = 0)$ response in oblique seas with PNE = 0.368:

$$\Sigma_{\text{m-EDW}} = \begin{bmatrix} 1 & -0.91 & 0.24 & -0.94 & 0.76 \\ -0.91 & 1 & 0.19 & 0.71 & -0.96 \\ 0.24 & 0.19 & 1 & -0.56 & -0.45 \\ -0.94 & 0.71 & -0.56 & 1 & -0.49 \\ 0.76 & -0.96 & -0.45 & -0.49 & 1 \end{bmatrix} \quad \text{rank}(\Sigma_{\text{m-EDW}}) = 2 \quad \Sigma_{\text{m-EDW}} - \Sigma_{\text{MCS}} = \begin{bmatrix} 0 & -0.36 & 0.32 & -0.09 & 0.04 \\ -0.36 & 0 & -0.04 & 0.23 & -0.19 \\ 0.32 & -0.04 & 0 & -1.06 & -0.61 \\ -0.09 & 0.23 & -1.06 & 0 & -0.02 \\ 0.04 & -0.19 & -0.61 & -0.02 & 0 \end{bmatrix} \quad \text{(A.14)}$$

$$\Sigma_{\text{m-CRRW}} = \begin{bmatrix} 1 & -0.43 & -0.20 & -0.77 & 0.66 \\ -0.43 & 1 & -0.28 & -0.16 & -0.89 \\ -0.20 & -0.28 & 1 & 0.53 & 0.20 \\ -0.77 & -0.16 & 0.53 & 1 & -0.10 \\ 0.65 & -0.89 & 0.20 & -0.10 & 1 \end{bmatrix} \quad \text{rank}(\Sigma_{\text{m-CRRW}}) = 5 \quad \Sigma_{\text{m-CRRW}} - \Sigma_{\text{MCS}} = \begin{bmatrix} 0 & 0.12 & -0.12 & 0.09 & -0.06 \\ 0.12 & 0 & -0.51 & -0.64 & -0.12 \\ -0.12 & -0.51 & 0 & 0.02 & 0.04 \\ 0.09 & -0.64 & 0.02 & 0 & 0.38 \\ -0.06 & -0.12 & 0.04 & 0.38 & 0 \end{bmatrix}$$

$$\Sigma_{\text{DLG}} = \begin{bmatrix} 1 & -0.68 & -0.06 & -0.81 & 0.74 \\ -0.68 & 1 & -0.07 & 0.38 & -0.83 \\ -0.06 & -0.07 & 1 & 0.52 & 0.11 \\ -0.81 & 0.38 & 0.52 & 1 & -0.50 \\ 0.74 & -0.83 & 0.11 & -0.50 & 1 \end{bmatrix} \quad \text{rank}(\Sigma_{\text{DLG}}) = 5 \quad \Sigma_{\text{DLG}} - \Sigma_{\text{MCS}} = \begin{bmatrix} 0 & -0.13 & 0.02 & 0.05 & 0.02 \\ -0.13 & 0 & -0.30 & -0.10 & -0.06 \\ 0.02 & -0.30 & 0 & 0.02 & -0.05 \\ 0.05 & -0.10 & 0.02 & 0 & -0.03 \\ 0.02 & -0.06 & -0.05 & -0.03 & 0 \end{bmatrix}$$

$$\Sigma_{\text{MCS}} = \begin{bmatrix} 1 & -0.55 & -0.08 & -0.85 & 0.72 \\ -0.55 & 1 & 0.23 & 0.48 & -0.77 \\ -0.08 & 0.23 & 1 & 0.51 & 0.16 \\ -0.85 & 0.48 & 0.51 & 1 & -0.47 \\ 0.72 & -0.77 & 0.16 & -0.47 & 1 \end{bmatrix} \quad \text{rank}(\Sigma_{\text{MCS}}) = 5 \quad \begin{array}{c} |\det(\Sigma_{\text{m-EDW}} - \Sigma_{\text{MCS}})| = 0.023 \\ |\det(\Sigma_{\text{m-CRRW}} - \Sigma_{\text{MCS}})| = 0.001 \\ |\det(\Sigma_{\text{DLG}} - \Sigma_{\text{MCS}})| = 2.68e\text{-}6 \end{array}$$

References

Adegeest, L.J.M., Braathen, A., Løseth, R.M., 1998. Use of non-linear sea-loads simulations in design of ships. In: Practical Design of Ships and Mobile Units. Practical Design of Ships and Mobile Units. Practical Design of Ships and Mobile Units. pp. 53–58. http://dx.doi.org/10.1016/S0928-2009(98)80138-8.

Alford, L.K., 2008. Estimating Extreme Responses using a Non-Uniform Phase Distribution (Ph.D. thesis). The University of Michigan.

Alfred Mohammed, E., Benson, S.D., Hirdaris, S.E., Dow, R.S., 2016. Design safety margin of a 10,000 TEU container ship through ultimate hull girder load combination analysis. Mar. Struct. (ISSN: 0951-8339) 46, 78–101. http://dx.doi.org/10.1016/j.marstruc.2015.12.003.

Alfred Mohammed, E., Chan, H.S., Hirdaris, S.E., 2012. Global wave load combinations by cross-spectral methods. Mar. Struct. (ISSN: 0951-8339) 29 (1), 131–151. http://dx.doi.org/10.1016/j.marstruc.2012.10.005.

American Bureau of Shipping, 2005. Guidance Notes on 'Safehull-Dynamic Loading Approach' for Container Carriers. Technical Report, April.

American Bureau of Shipping, 2016. Guidance Notes on Selecting Design Wave by Long Term Stochastic Method. Technical Report.

Bureau Veritas, 2017. Rules for the classification of naval ships. June.

Bureau Veritas, 2018a. Rules for the classification of steelships. July.

Bureau Veritas, 2018b. Guidance Note for Structural Assessment of Passenger Ships and Ro-Ro Passenger Ships. January.

ClassNK, 2013. Rules for the Survey and Construction of Steel Ships. Part CRS-T.

Dietz, J.S., 2004. Application of Conditional Waves as Critical Wave Episodes on Marine Structures (Ph.D. thesis). Technical University of Denmark.

DNV-GL, 2018. Class Guideline. Technical Report DNVGL-CG-0130, DNV-GL, January.

Drummen, I., Wu, M.K., Moan, T., 2009. Numerical and experimental investigations into the application of response conditioned waves for long-term nonlinear analyses. Mar. Struct. (ISSN: 0951-8339) 22 (3), 576–593. http://dx.doi.org/10.1016/j.marstruc.2008.12.002.

Feld, G., Jonathan, P., Randell, D., 2019. On the estimation and application of directional design criteria. In: Proceedings of the 38th International Conference on Ocean, Offshore and Arctic Engineering.

Ferry-Borges, J., Castanheta, M., 1971. Lisbon: Laboratoria nacional de engenhera civil. Struct. Saf.

Friis-Hansen, P., Nielsen, L.P., 1995. On the new wave model for the kinematics of large ocean waves. In: Proceedings of the 14th International Conference on Offshore Mechanics and Arctic Engineering. Copenhagen, Denmark, pp. 14–24.

Horn, G.E., Arima, T., Baumans, P., Bøe, A., Ocakli, H., 2013. IACS Summary of the IMO GBS and the Harmonised Common Structural Rules. Technical Report, TSCF 2013 Shipbuilders Meeting.

Huang, W., Moan, T., 2008. Analytical method of combining global longitudinal loads for ocean-going ships. Probab. Eng. Mech. (ISSN: 0266-8920) 23 (1), 64–75. http://dx.doi.org/10.1016/j.probengmech.2007.10.005.

IACS, 2018. NR606 Common Structural Rules for Bulk Carriers and Oil Tankers. Technical Report, July.

Kim, D.-H., 2012. Design Loads Generator: Estimation of Extreme Environmental Loadings for Ship and Offshore Applications (Ph.D. thesis). The University of Michigan.

Kring, D.C., Milewski, W.M., Fine, N.E., 2004. Validation of a NURBS-based BEM for multihull ship seakeeping. In: 25th Symposium on Naval Hydrodynamics St. John's. Newfoundland and Labrador, Canada.

Lindgren, G., 1970. Some properties of a normal process near a local maximum. Ann. Math. Stat. 41 (6), 1870–1883.

Lloyd's Register, 2014. Common Structural Rules for Bulk Carriers and Oil Tankers. Technical Report, Lloyd's Register, January.

Lloyd's Register, 2017. Rules for the Classification of Trimarans. Technical Report, Lloyd's Register.

Ochi, M.K., 1990. Applied Probability & Stochastic Processes in Engineering & Physical Sciences. In: Wiley Series in Probability and Mathematical Sciences.

Piscopo, V., Scamardella, A., 2019. Sensitivity analysis of hull girder reliability in intact condition based on different load combination methods. Mar. Struct. (ISSN: 0951-8339) 64, 18–34. http://dx.doi.org/10.1016/j.marstruc.2018.10.009.

Seyffert, H.C., Kana, A.A., 2019. Evaluation of an equivalent design wave method to define lifetime combined loading scenarios for trimarans. In: Proceedings of the 38th International Conference on Ocean, Offshore and Arctic Engineering.

Seyffert, H.C., Troesch, A.W., Collette, M.D., 2019. Combined stochastic lateral and in-plane loading of a stiffened ship panel leading to collapse. Mari. Struct.

Seyffert, H.C., Troesch, A.W., Knight, J.T., Kring, D.C., 2018. Probabilistic assessment of combined loads for trimarans. In: International Marine Design Conference. Helsinki, Finland.

Smith, S., 2002. Digital Signal Processing: A Practical Guide for Engineers and Scientists, Vol. 1. Newnes.

Taylor, P.H., Jonathan, P., Harland, L.A., 1997. Time domain simulation of jack-up dynamics with the extremes of a Gaussian process. J. Vib. Acoust. Trans. ASME 119, 624–628.

Torhaug, R., 1996. Extreme Response of Nonlinear Ocean Structures: Identification of Minimal Stochastic Wave Input for Time-domain Simulation (Ph.D. thesis). Stanford University.

Tromans, P.S., Anaturk, A.R., Hagemeijer, P., 1991. A new model for the kinematics of large ocean waves - application as a design wave. In: Proceedings, 1st Internationl Offshore and Polar Engineering Conference, Vol. III. ISOPE. pp. 64–71.

Turkstra, C.J., 1970. Theory of Structural Design Decisions Study No. 2. Solid Mechanics Division, University of Waterloo, Ontario, Canada.

Wen, Y.K., 1993. Reliability-based design under multiple loads. Struct. Saf. (ISSN: 0167-4730) 13 (1), 3–19. http://dx.doi.org/10.1016/0167-4730(93)90044-2, Special Issue on Combinations of Actions to Structures.